Wegener Center for Climate and Global Change
University of Graz
Leechgasse 25, A-8010 Graz, Austria

Atmospheric Remote Sensing and Climate System Research Group
CHAMPCLIM Project Report

WegCenter/UniGraz Technical Report for FFG-ALR No. 3/2006

FFG-ALR study:

CHAMPCLIM – Radio Occultation Data Analysis Advancement and Climate Change Monitoring Based on the CHAMP/GPS Experiment

[Contract No: ASAP-WV-203/05 – September 2005]

MONITORING REPORT

[WP4: MONITOR]

CHAMP Radio Occultation Based Climatologies for Global Monitoring of Climate Change

U. Foelsche, M. Borsche, A.K. Steiner, B. Pirscher, B.C. Lackner, A. Gobiet, and G. Kirchengast

Wegener Center for Climate and Global Change (WegCenter),
University of Graz, Graz, Austria

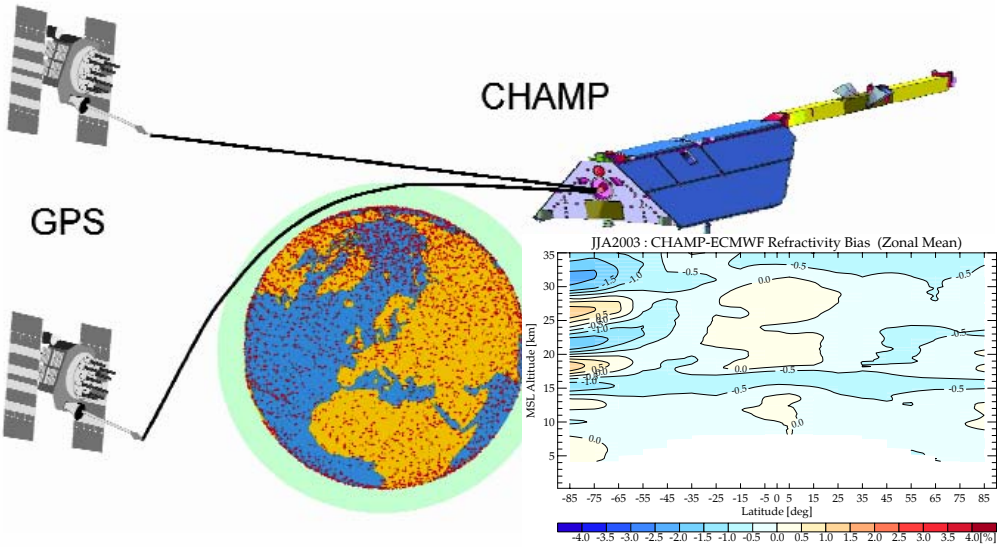

February 2006

Table of Contents

1 INTRODUCTION AND CONTEXT 1

2 CLIMATE MONITORING WITH RADIO OCCULTATION 3

2.1 Properties of Radio Occultation Data 3

2.1.1 Long-Term Stability due to Intrinsic Self-Calibration 4

2.1.2 Spatial and Temporal Coverage 4

2.2 Atmospheric Parameters for Climate Monitoring 5

2.3 The Role of the CHAMPCLIM Project 7

2.3.1 RO Data Processing Advancements for Optimizing Climate Utility 7

2.3.2 RO Data and Algorithms Validation Based on CHAMP/GPS Data 7

2.3.3 Global RO Based Climatologies for Monitoring Climate Change 8

3 SAMPLING ERRORS 9

3.1 Selective Sampling in Dry Regions 9

3.2 Temporal and Spatial Undersampling 10

3.3 Local Time Sampling 11

4 RO BASED CLIMATOLOGIES 15

4.1 Error Estimates 15

4.1.1 Estimation of the Observational Error 15

4.1.2 Estimation of the Sampling Error 18

4.2 Seasonal CHAMP Temperature Climatologies 19

4.3 CHAMPCLIM Multi-Parameter Fields 29

4.4 Special CHAMPCLIM Products 31

4.4.1 Tropopause Parameters 31

4.4.2 Principal Component Analysis (PCA) 33

5 CONCLUSIONS AND OUTLOOK 39

Acknowledgments 39

REFERENCES 41

APPENDIX A: MONTHLY CLIMATOLOGIES FOR A FULL YEAR 45

List of Acronyms

ASA	Austrian Space Agency
CHAMP	CHAllenging Minisatellite Payload
CHAMPCLIM	Radio Occultation Data Analysis Advancement and Climate Change Monitoring based on the CHAMP/GPS Experiment – research project in the ASAP program carried out by WegCenter/UniGraz
COSMIC	Constellation Observing System for Meteorology, Ionosphere, and Climate
DJF	Winter season (December, January, February)
ECHAM5	Fifth-generation atmospheric general circulation model developed from the ECMWF atmospheric model (EC) at the Max Planck Institute for Meteorology, Hamburg (HAM)
ECMWF	European Centre for Medium-range Weather Forecasts
EGOPS	End-to-end GNSS Occultation Performance Simulator
EGOPS/CCR	CHAMPCLIM Retrieval – software tool for the retrieval of CHAMP RO data based on EGOPS
ENVISAT	ENVIronment SATellite (of ESA)
ESA	European Space Agency
EUMETSAT	EUropean organisation for the exploitation of METeorological SATellites
GFZ	GeoForschungsZentrum Potsdam
GNSS	Global Navigation Satellite System (generic term for GPS, GALILEO, GLONASS)
GOMOS	Global Ozone Monitoring by Occultation of Stars (on ENVISAT)
GPS	Global Positioning System (USA)
GPS/MET	GPS METeorology – "proof-of-concept" experiment for the GPS RO technique on MicroLab-1 in 1995
GRAS	Global navigation satellite system Receiver for Atmospheric Sounding (on MetOp)
IGAM	Institute for Geophysics, Astrophysics, and Meteorology, University of Graz, Austria
IPCC	Intergovernmental Panel on Climate Change
JJA	Summer season (June, July, August)
LEO	Low Earth Orbit
MAM	Spring season (March, April, May)
MetOp	Meteorological Operational satellite
MIPAS	Michelson Interferometer for Passive Atmospheric Sounding (on ENVISAT)
MSU	Microwave Sounding Unit
NWP	Numerical Weather Prediction
RO	Radio Occultation
SAC-C	Satélite de Aplicaciones Científicas-C
SON	Fall season (September, October, November)
UniGraz	University of Graz, Graz, Austria
U.S.	United States of America
WegCenter	Wegener Center for Climate and Global Change, UniGraz

List of Symbols

σ	Standard deviation
e	Partial pressure of water vapor in the atmosphere
H_{strat}	Scale height of the refractivity error increase in the stratosphere domain
k_1, k_2	Constants in refractivity formula ($k_1 = 77.60\ \mathrm{K\,hPa^{-1}}$, $k_2 = 3.73 \cdot 10^5\ \mathrm{K^2\,hPa^{-1}}$)
L	Vertical error correlation length
L1, L2	GPS L-band signals
N	Refractivity ($N = 10^6(n - 1)$)
n	Refractive index
n_{occ}	Number of occultation profiles
p	Pressure
s	(Relative) Standard deviation profile
s_0	(Relative) standard deviation at about 1 km altitude
s_{utls}	(Relative) standard deviation in the upper troposphere/lower stratosphere
T	Temperature
T_{dry}	Dry temperature
z	Altitude
z_p	Pressure Altitude
$z_{stratbot}$	Bottom level of the “stratosphere domain”
$z_{troptop}$	Top level of the “troposphere domain”

1 Introduction and Context

Increasing evidence suggests that the Earth's climate is significantly influenced by human activities. While there is little doubt that the Earth's surface temperature has risen by about 0.6 K during the 20th century, the amount and even the existence of temperature trends in the troposphere are still under debate. Additional high quality observations of the atmosphere are therefore particularly required in this context. The Global Navigation Satellite System (GNSS) radio occultation (RO) technique has the potential to substantially contribute to this scientific challenge.

The special climate utility of RO data arises from their long-term stability due to their self-calibrated nature. Atmospheric profiles obtained by RO active limb sounding are not derived from intensity or radiance measurements but from Doppler shift (phase change) profiles requiring no external calibration and only short-term phase measurement stability over the order of 1 min of RO event duration. The latter is guaranteed by very stable oscillators onboard the transmitter and receiver satellites. With each single RO event intrinsically calibrated this way, and using consistent data processing, the long-term stability of any derived multi-year climate dataset is ensured. Data from different sensors and different occultation missions can be combined without need for inter-calibration and overlap, as long as the same data processing scheme is used. Accurate phase change measurements are the basis of high quality retrievals of bending angles and the atmospheric variables refractivity, density, pressure, geopotential height, temperature, and humidity.

The German/U.S. research satellite CHAMP was launched in July 2000 into low Earth orbit (LEO). Since March 2002, after an initial phase with an increasing number of RO events measured, it continuously records about 230 RO profiles per day (*Wickert et al.*, 2001; 2004). Out of these ~230 daily profiles, about 160 can be successfully processed to phase delays and are of sufficient data quality; ~150 of these pass the quality checks during the WegCenter atmospheric profiles retrieval. The CHAMP mission is expected to last until 2007, CHAMP RO data thus provide the first opportunity to create RO based climatologies for a multi-year period of > 5 years.

The overall aim of the CHAMPCLIM project is to contribute to the best possible exploitation of CHAMP RO data, in particular for climate monitoring. This "Monitoring Report" describes the results of work package (WP) 4 of the project: Global RO based climatologies for monitoring climate change. In section 2 we summarize the properties of RO data, with respect to the CHAMP mission and climate monitoring. Furthermore, we consider appropriate atmospheric parameters for climate monitoring. In section 3 we concentrate on different sampling errors, which are of particular importance for RO based climatologies. Seasonal climatologies, corresponding error estimates, and some special climate monitoring products are discussed in section 4, followed by conclusions and outlook in section 5.

The report is complemented by an appendix, Appendix A, which presents monthly-mean, zonal-mean climatologies together with the corresponding error estimates for a complete year. This overview serves as a small atlas for readers with closer interest in the subject. By way of a full example year (year 2003) it illustrates in more detail the wealth of information in the CHAMPCLIM climatology products derived from CHAMP RO observations.

2 Climate Monitoring with Radio Occultation

The provision of accurate, long-term consistent data to sustain and expand the observational foundation for climate studies is one of the high priority areas for action to improve the ability to detect, attribute and understand climate variability and change (*IPCC*, 2001). While there is little doubt that the Earth's surface temperature has risen by about 0.6 K during the 20th century (*IPCC*, 2001), our knowledge about the temperature evolution in the free atmosphere is still very limited. Traditional satellite derived data records like those from the microwave sounding units (MSU) on board NOAA polar orbiting satellites are degraded by problems like instrument and orbit changes, calibration problems, instrument drifts, and lacking vertical resolution (*Anthes et al*., 2000).

Because of these shortcomings, the amount of temperature trends in the troposphere is still under debate (e.g., *Christy and Spencer*, 2003; *Vinnikov and Grody*, 2003; *Mears et al.*, 2003; *Fu et al.*, 2004; *Bengtsson et al.*, 2004).

A promising climate monitoring tool which can overcome these problems is the Global Navigation Satellite System (GNSS) Radio Occultation (RO) technique. For detailed descriptions on this satellite-to-satellite active limb sounding method and its potential see, e.g., *Ware et al*. (1996), *Kursinski et al*. (1997), *Steiner et al*. (2001), and *Hajj et al*. (2002); for the general utility of occultation methods for probing atmosphere and climate see, e.g., *Kirchengast* (2004).

Sensing of the Earth's atmosphere with the RO method was first successfully demonstrated with the GPS Meteorology (GPS/MET) experiment within 1995–1997 (*Kursinski et al.*, 1996; *Ware et al*., 1996; *Rocken et al.*, 1997; *Steiner et al*., 1999; www.cosmic.ucar.edu/gpsmet). The German/U.S. research satellite CHAMP (CHAllenging Minisatellite Payload for geoscientific research) was launched in July 2000 and since March 2002 it continuously records about 200 RO profiles per day (*Wickert et al.*, 2001; 2004; www.gfz-potsdam.de/champ). The CHAMP mission is expected to last at least until 2007. CHAMP RO data thus provide the first opportunity to create RO based climatologies on a longer multi-year term.

2.1 Properties of Radio Occultation Data

Accurate phase change measurements are the basis of high quality retrievals of bending angles and the atmospheric variables refractivity, density, pressure, geopotential height, temperature, and humidity.

Highest quality of RO observations is achieved in the upper troposphere/lower stratosphere region (UTLS), a domain re-acting very sensitive to climate change, where expected trends in atmospheric parameters are particularly large (e.g., *Foelsche et al*., 2005). Compared to weather analyses CHAMP RO temperature data show an ensemble mean agreement of <0.4 K between 10 km and 35 km height with a standard deviation of ~1 K at 10 km increasing to ~2 K at 30 km height (*Wickert et al*., 2004).

The active use of L-band signals with wavelengths of 19.0 cm and 24.4 cm (in case of GPS), respectively, allows for measurements during day and night and for penetration of clouds.

2.1.1 Long-Term Stability due to Intrinsic Self-Calibration

Regarding climate monitoring, the long-term stability of RO data is of particular importance (see, e.g., *Leroy et a*l., 2006). It can be achieved since atmospheric profiles are not derived from absolute values (phase delays) but from Doppler shift (phase change) profiles. Therefore, RO measurements require no external calibration and only short-term measurement stability over the occultation event duration (1 – 2 min), which is guaranteed by very stable oscillators onboard the GNSS satellites. Given this "self-calibration", data from different sensors and different occultation missions can be combined without need for inter-calibration and overlap, as long as the same data processing scheme is used.

The long-term stability of RO data could not be tested so far due to the lack of long-time observations. An intercomparison study by *Hajj et al*. (2004) based on data from CHAMP and SAC-C (Satélite de Aplicaciones Científicas-C), however, showed a remarkable consistency of the data obtained from these two different satellites, with temperature profiles found consistent to 0.1 K in the mean between 5 km and 15 km.

While CHAMP and SAC-C are equipped with very similar receivers, leaving the possibility of common systematic errors, future RO missions will help assess whether these results can also be obtained with data from completely different receivers, like the GRAS instrument (GNSS Receiver for Atmospheric Sounding) onboard MetOp (Meteorological Operational satellite, launch expected for June 2006) (*Loiselet et al*., 2000).

2.1.2 Spatial and Temporal Coverage

The number of RO events depends primarily on the number of available transmitters and receivers. A single receiver in low Earth orbit (LEO), which is capable of tracking GPS signals during setting occultations (like on CHAMP) can collect ~250 RO profiles per day (for a nominal constellation of 24 GPS satellites). LEO satellites with an additional antenna for rising events can achieve twice that amount. The 6 COSMIC satellites (Constellation Observing System for Meteorology, Ionosphere, and Climate) (*Wu et al*., 2005), which are scheduled to be launched in March 2006, can be expected to obtain ~3000 setting and rising occultations per day, providing a valuable database for RO based climatologies (*Rocken et a*l., 2000). With the upcoming European Galileo system (nominal constellation of 30 satellites), the number of transmitters will more than double; the operational status of Galileo is expected to be reached in 2008/09.

The geographic distribution of the RO events depends on the geometry of the satellite orbits. Global coverage can only be obtained with a high-inclination orbit of the LEO satellite. This orbit geometry leads, however, to a high RO event density at high latitudes with comparatively fewer events at low latitudes. Figure 1 shows, as an example for this situation, the typical coverage of CHAMP RO data during one season. LEO satellites with a low inclination orbit, on the other hand, provide a better sampling at low latitudes, but do not reach global coverage.

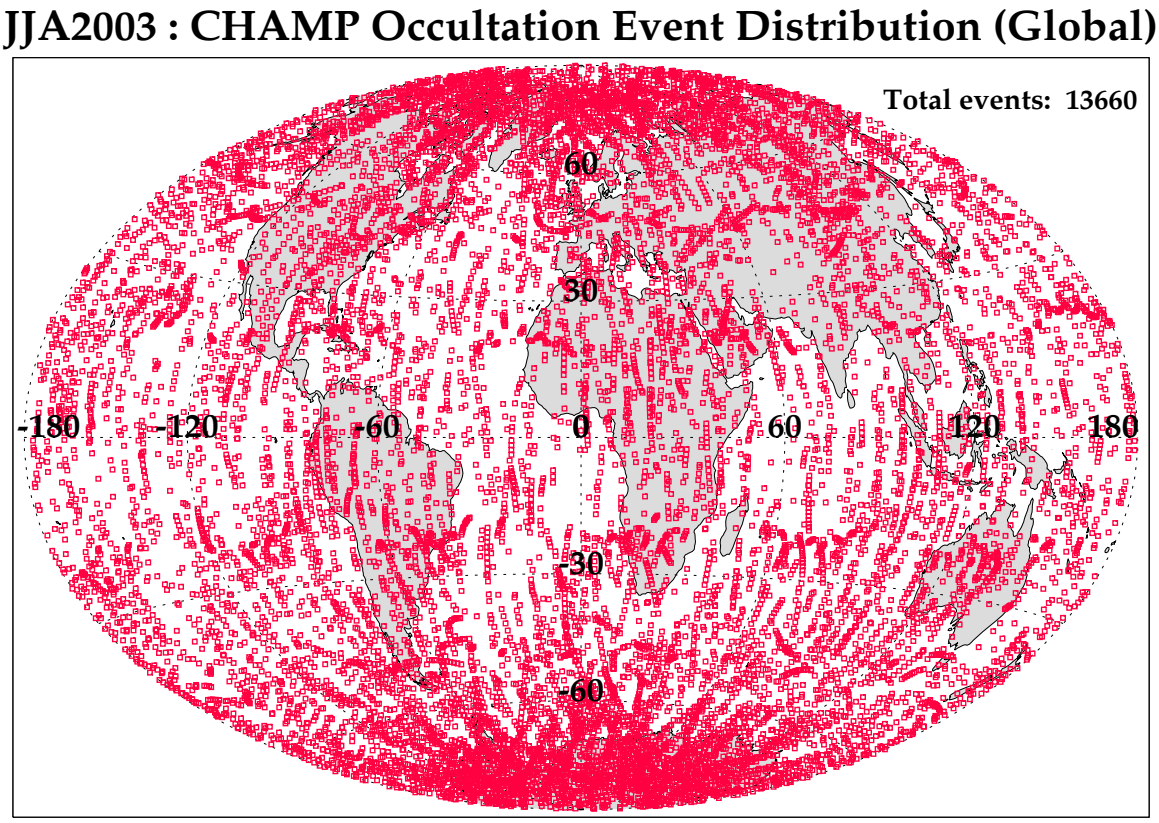

Fig. 1. Geographic distribution of 13553 CHAMP RO events during the northern summer season (June-July-August) 2003 (CHAMP orbit inclination = 87.3°).

The LEO orbit geometry determines furthermore the local times of the RO events. Satellites in sun-synchronous orbits, like MetOp, always cross the equator at the same local times. As a consequence, MetOp RO events will be clustered around 9:30 a.m. and 9:30 p.m. local time, respectively. All non-sun-synchronous LEO orbits are subject to a drift in equator-crossing time. The resulting local time drift of the CHAMP RO data is about 1 hour in 11 days.

When attempting to build RO climatologies, we have to consider that any uneven spatial and temporal sampling of the "true" evolution of the atmospheric fields can lead to sampling errors (see section 3).

2.2 Atmospheric Parameters for Climate Monitoring

In contrast to applications of RO data in numerical weather prediction, where the focus is clearly on RO products which are as close as possible to the raw measurements (e.g., *Poli* 2006), ideal parameters for climate monitoring are those which change most in a changing climate. Refractivity (*Vedel and Stendel*, 2003) and geopotential height (*Leroy*, 1997) have recently been identified as good indicators for climate change.

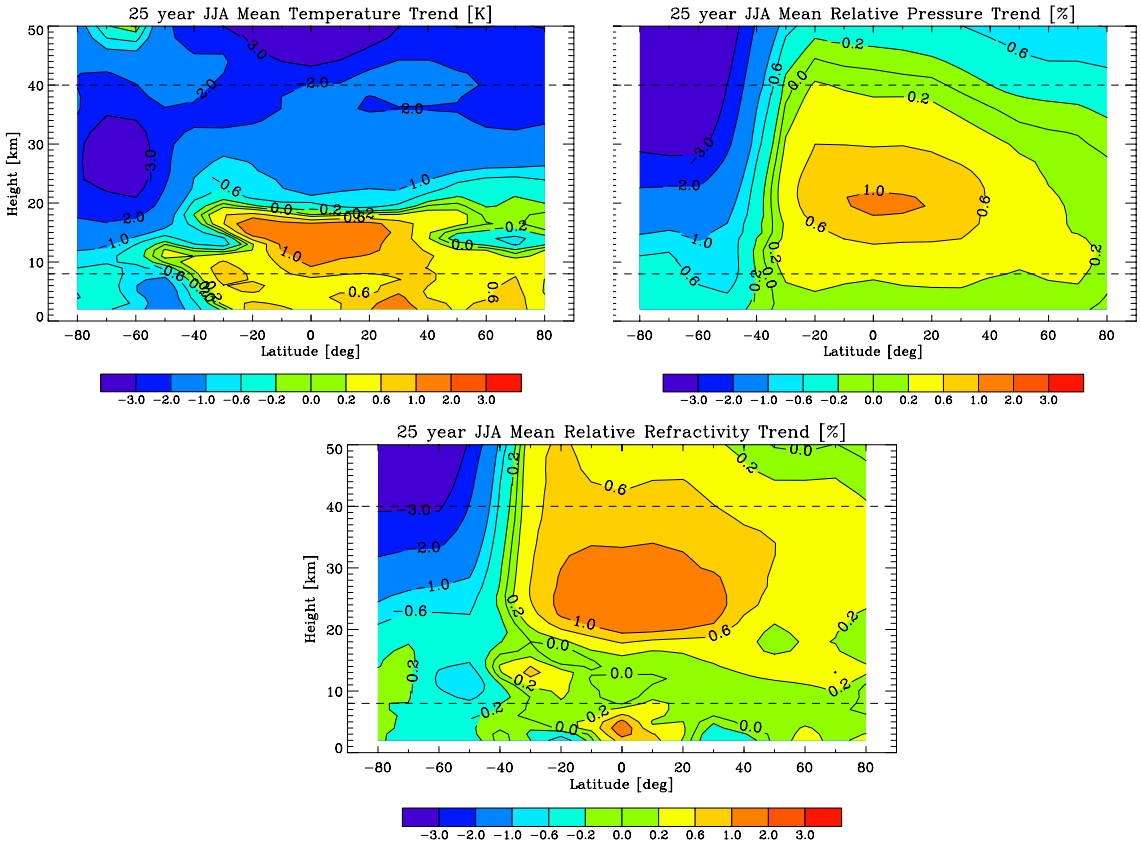

Fig. 2. Trends in atmospheric parameters over the 25-year period 2001–2025 as modeled with ECHAM5 (IS92a emission scenario with CO_2 concentration doubling between 1990 and 2100). Temperature trends (upper left panel), relative pressure trends (upper right panel), and relative trends in microwave refractivity (lower panel). From *Foelsche et al.* (2006).

Results from climate model runs can be used as indicators for expected trends in atmospheric parameters (*Foelsche et al.*, 2006). As an example, Figure 2 shows 25-year-trends (2001–2025) of temperature, pressure, and refractivity as results of runs of the ECHAM5 model (*Roeckner et al.*, 2003) in "middle atmosphere mode" with anthropogenic forcing. For this experiment, the vertical domain of the model was extended to 80 km. A dominant feature, which is only partly visible in "normal" climate model runs with a vertical domain up to 30 km, is the pronounced cooling in the stratosphere. Given the accuracy of RO data in the lower stratosphere it is likely that stratospheric "global cooling" will be the first consequence of anthropogenic climate change that can be detected with the aid of the RO technique.

An interesting feature of Fig. 2 is the lack of change in refractivity in the upper tropical troposphere. Microwave refractivity N is related to temperature T, total pressure p, and water vapor partial pressure e, via (*Smith and Weintraub*, 1953):

$$N = k_1 \frac{p}{T} + k_2 \frac{e}{T^2} \qquad (1)$$

where k_1 is 77.6 K/hPa and k_2 is $3.73 \cdot 10^5$ K^2/hPa. When atmospheric humidity is small, the second term on the right-hand-side of Eq. 1 can be neglected. We immediately see that in this case, the same relative increase in T and p will result in no change in refractivity. Figure 2 shows that different atmospheric parameters are sensitive in different regions of the

atmosphere. Climate monitoring with RO data should therefore, in principle, comprise all parameters that can be retrieved with the RO technique.

2.3 The Role of the CHAMPCLIM Project

The overall aim of CHAMPCLIM is to contribute to the best possible exploitation of CHAMP RO data, in particular for climate monitoring. The results of this project provide a starting point for RO based climatologies, which can be continuously expanded with data from other RO missions. The main objectives of CHAMPCLIM and some initial results have been described in *Foelsche et al.* (2005). Part I of the CHAMPCLIM project has been completed in November 2004. Main scientific objectives of CHAMPCLIM-Part I were the following work areas (each carried out within a project work package):

- RO data and algorithms validation based on CHAMP/GPS data
- RO data processing advancements for optimizing climate utility

The main results from these two work areas are briefly summarized in the sections 2.3.1 and 2.3.2, respectively, below. The main objective of CHAMPCLIM-Part II is:

- Global RO based Climatologies for Monitoring Climate Change

2.3.1 RO Data Processing Advancements for Optimizing Climate Utility

The essential outcome of this work was a robust CHAMPCLIM retrieval scheme (WegCenter/CCRv2), building on the EGOPS4 software tool (*Kirchengast et al*., 2002) and a reasonable error characterization for CHAMP/GPS RO data in meeting the aim to improve the maturity and utility of the data products especially for climatological purposes. Main aspects of WegCenter/CCRv2 are:

- Geometric optics retrieval. The implementation of a wave optics retrieval scheme for the troposphere is planned for CCRv3.
- Ionospheric correction via linear combination of bending angles.
- Transparent input of a priori information via statistical optimization of bending angles. For the results shown here, ECMWF (European Centre for Medium-range Weather Forecasts) data have been used for background bending angles.
- No further initialization of the hydrostatic integral.
- Dry air retrieval (e.g., *Syndergaard*, 1999). A 1D-Var retrieval for humidity and temperature in the troposphere is planned for CCRv3.

Further details of the CCRv2 retrieval can be found in a dedicated CHAMPCLIM report (*Steiner et al*., 2004) as well as in *Gobiet and Kirchengast* (2004), and *Borsche et al.* (2006a). Results of a related error analysis can be found in *Steiner and Kirchengast* (2005) and of an error analysis using CHAMP refractivity profiles in *Steiner et al*. (2006).

2.3.2 RO Data and Algorithms Validation Based on CHAMP/GPS Data

The WegCenter/CCRv2 retrieval scheme was validated against a modeled atmosphere in an end-to-end simulation study, the GFZ operational RO retrieval scheme, numerical weather prediction analyses from ECMWF, and remote-sensing instruments onboard ENVISAT (MIPAS and GOMOS). Results of these validation studies can be found in another CHAMPCLIM report (*Gobiet et al*., 2004) and in *Gobiet et al*. (2005a).

2.3.3 Global RO Based Climatologies for Monitoring Climate Change

Within CHAMPCLIM-Part II the WegCenter/CCR retrieval has been further advanced, the current version (CCRv2.3) is described in detail in the CHAMPCLIM report by *Borsche et al.* (2006b). The main work of CHAMPCLIM-Part II focused on building climatologies and on investigating different error sources, especially sampling errors (see section 3).

Based on the validated datasets obtained by advanced retrievals of atmospheric parameters from CHAMP RO data, we build climatologies in two different ways. In a first approach, we perform direct (model independent) monitoring of the evolution of climatological atmospheric fields through binning and averaging of RO profiles (see section 4).

In a second approach we assimilate CHAMP RO-derived refractivities into ECMWF short term forecast fields (via 3D-Var) to obtain global climate analyses with higher horizontal resolution. Results of this approach are the focus of the CHAMPCLIM report by *Löscher et al*. (2006). This line of analyzed climatologies will be further advanced in the future in co-operation with the EUMETSAT/MetOp GRAS Satellite Application Facility (GRAS-SAF) at DMI Copenhagen, Denmark. The WegCenter's main future emphasis will be on direct reference climatologies with the potential to function as model-independent benchmark climate monitoring data.

The current record of RO occultations is still too short to actually monitor long-term trends, but comparison with other climatologies shows the value and the potential of the climatologies based on RO data.

3 Sampling Errors

The error due to spatial and temporal undersampling of the "true" evolution of atmospheric fields has been identified as a potential major error source for single-satellite climatologies with the aid of simulation studies (*Foelsche et al*., 2003). Even with perfect observations at the occultation locations the "measured" climatologies would differ from the "true" ones as the sampling through occultation events is discrete and not dense enough to capture the entire spatio-temporal variability of the atmosphere.

Under the assumption that the ECMWF analysis fields (4 time layers per day) sufficiently represent the "true" state of the atmosphere (including semi-diurnal cycles), we can estimate the sampling error by comparing climatologies derived from the "true" ECMWF profiles at the RO event locations with climatologies derived from the "true" 3D ECMWF fields using the complete field grid. The dry temperature results for the "testbed" season (JJA 2003), with the RO event distribution from Fig. 1, are displayed in Fig. 3. Above ~8 km the sampling error is, in general, < 0.5 K.

3.1 Selective Sampling in Dry Regions

In the lower troposphere at low and mid-latitudes, however, there is a large "warm" sampling error for dry temperatures. This feature can be interpreted as a selective "dry sampling error". The tracking of CHAMP signal and the geometric optics retrieval tends to stop at higher altitudes in moist compared to dry conditions. The lowest part of the RO ensembles is therefore biased towards dry conditions (with smaller refractivities), resulting in a systematic under-representation of the "true" mean refractivity (see Eq. 1, section 2.2). When the refractivities are converted to dry temperatures, this systematic error maps into warm-biased mean dry temperatures, via

$$T_{\mathrm{dry}} = k_1 \frac{p}{N}. \qquad (2)$$

This effect is most pronounced at low latitudes, where the event density is particularly low (see Fig. 1) due to the high inclination of the CHAMP satellite (87.3°). The implementation of a wave optics algorithm in the WegCenter/CCR retrieval will reduce this "dry sampling error", but it will remain an important error source for RO based climatologies at low latitudes below ~8 km. Operational CHAMPCLIM dry-retrieval climatologies will therefore be provided down to 8 km at low latitudes and down to 4 km at high latitudes. Starting at the poles down to 60° latitude the climatologies reach down to 4 km, the cut-off height then increases within 60° to 30° to reach 8 km height at low latitudes (within 30°N and 30°S). Within 60° to 30° the cut-off heights are 5 km (60°–50°), 6 km (50°–40°), and 7.5 km (40°–30°), respectively, reflecting the increasing relevance of moisture perturbation to dry temperature profiles towards low latitudes.

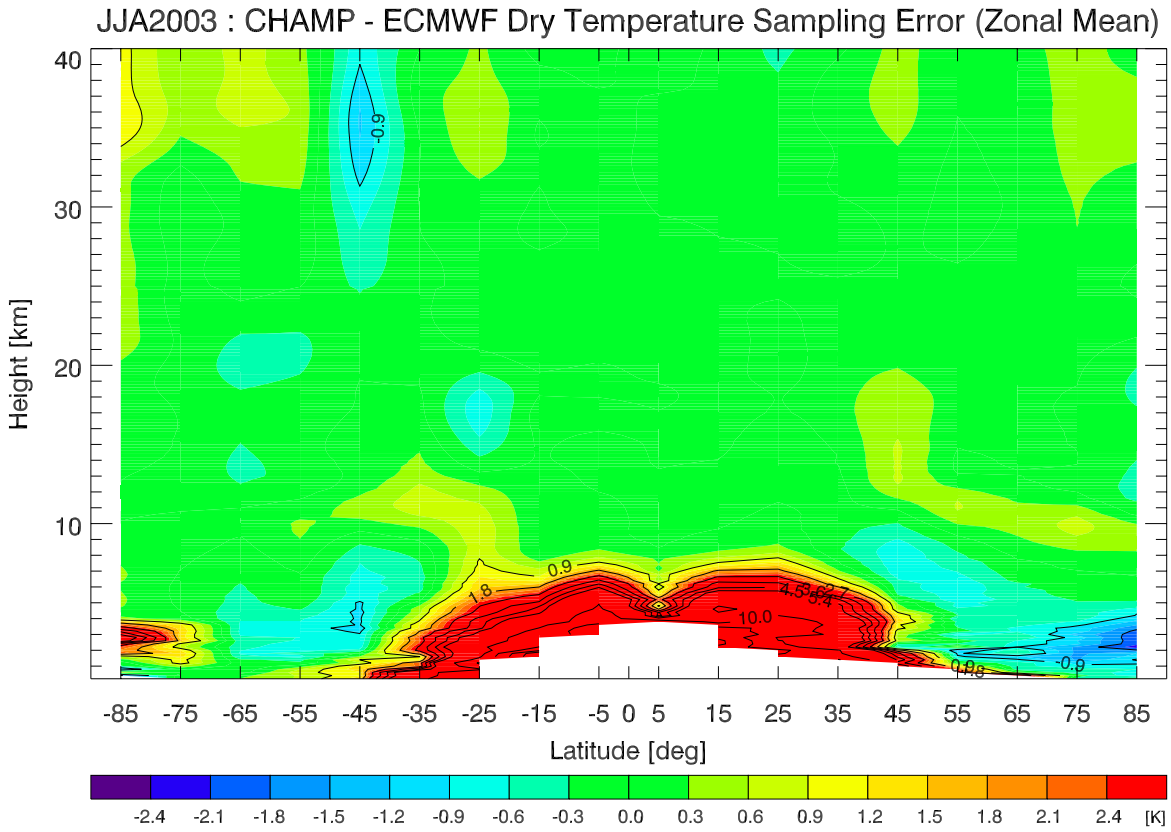

Fig. 3. Estimated CHAMP dry temperature sampling error for the (northern) summer season June-July-August (JJA) 2003. Seasonal and zonal means versus height above the ellipsoid with profiles sampled in 10° latitude bins.

3.2 Temporal and Spatial Undersampling

The geographical distribution of CHAMP RO events is determined by the geometry of the orbits of CHAMP and of the transmitting GPS satellites. The top panel of Fig. 4 shows a typical situation (June 2003) with comparatively well distributed RO events and corresponding small sampling errors, which are smaller than 0.5 K almost everywhere. Due to the high inclination of the CHAMP orbit (87.3°), the RO event density at high latitudes is higher than at low latitudes. Comparatively small temperature variations in these bins, however, prevent the sampling error from increasing dramatically.

In April 2003 (bottom panels of Fig. 4), the geometry of the satellite orbits leads to a remarkable clustering of RO events. The number of RO events in April is not much smaller than in June, but the number of independent bits of information is considerably smaller. The corresponding sampling error is thus significantly higher. A similar situation is encountered in April 2002, 2004 and 2005 (not shown). This problem cannot be easily overcome, since the distribution of RO events cannot be affected, but our strategy of co-monitoring of the sampling error provides a valuable means to identify time intervals and geographic regions that are subject to higher sampling errors.

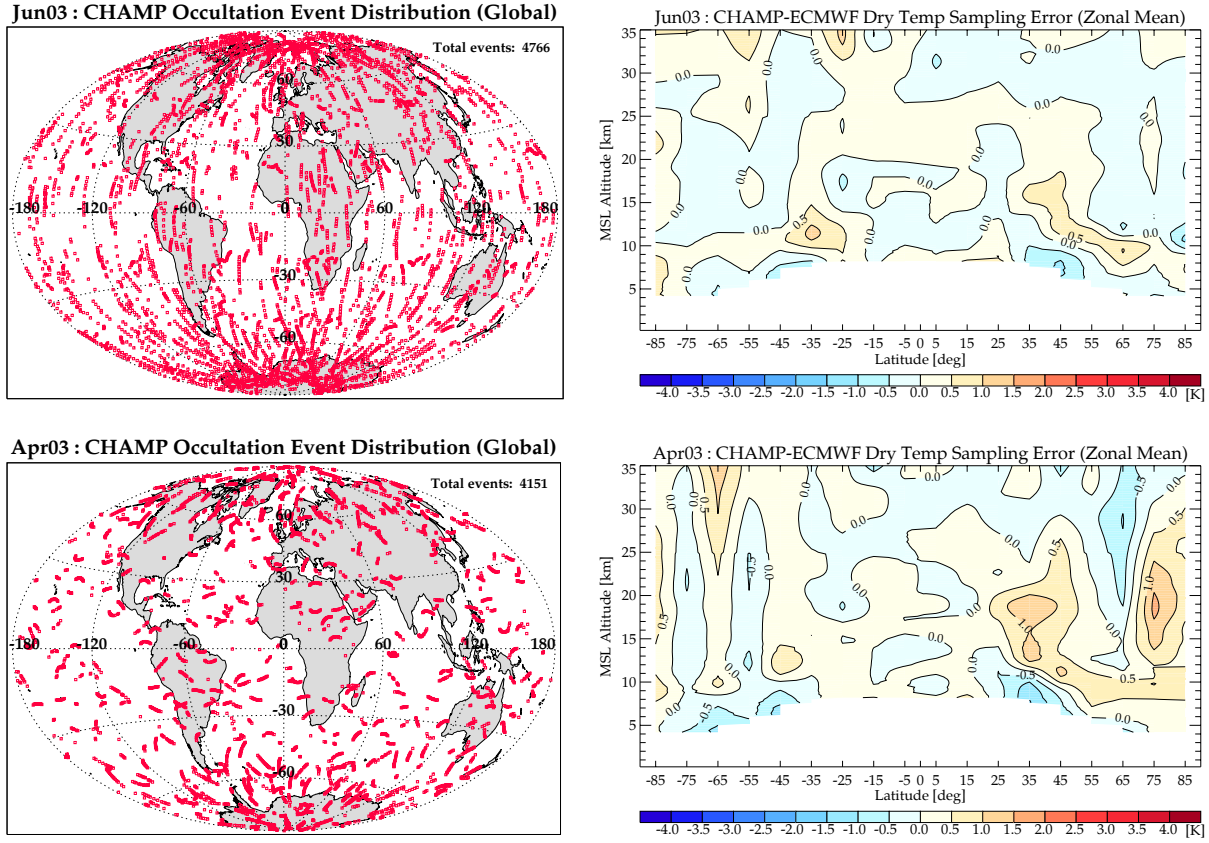

Fig. 4. Distribution of CHAMP RO events (left) and corresponding sampling error (right). Top: June 2003, bottom: April 2003.

3.3 Local Time Sampling

Concerning temperature data retrievals, the local time of the occultation events plays an essential role because of distinct daily temperature variations. A (slow) shift of the local time of occultation events could produce a temperature trend without physical relevance – simply caused by an inappropriate sampling interval.

The orbit geometry of the CHAMP satellite leads to a continuous change in equator crossing time with a rate of ~ 1 hour per 11 days. The RO events are clustered around the local times of the ascending and descending nodes. The distribution of CHAMP RO events for two months in 2003 is shown in Fig. 5: In May 2003 the peaks of the bimodal distribution of the histogram occur in the early morning (between 3 am and 6 am) and afternoon (3 pm to 6 pm). One month later, the peaks have moved ~ 3hrs "back" to near midnight (12 pm to 3 am) and near midday (12 am to 3 pm), respectively.

The uneven local time sampling decreases when seasonal means are considered. The distributions for two different seasons (Fig. 6) show, however, that even seasonal means (90-92 day period) are not yet fully sampling the diurnal cycle (the diurnal cycle is completely sampled within ~130 days).

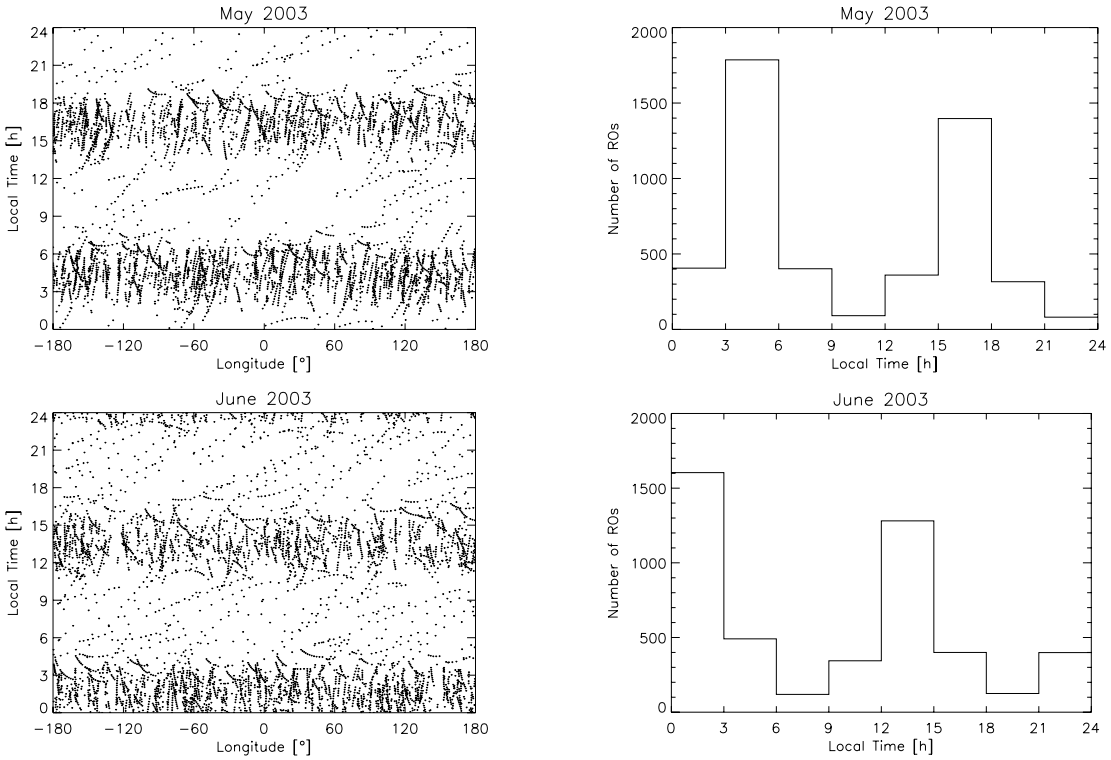

Fig. 5. Local time distribution of CHAMP RO events in May (top) and June 2003 (bottom). Left: Local time of RO events as a function of longitude. Right: Histogram of number of radio occultation events with three hour time intervals. A time shift of about three hours per month is clearly visible.

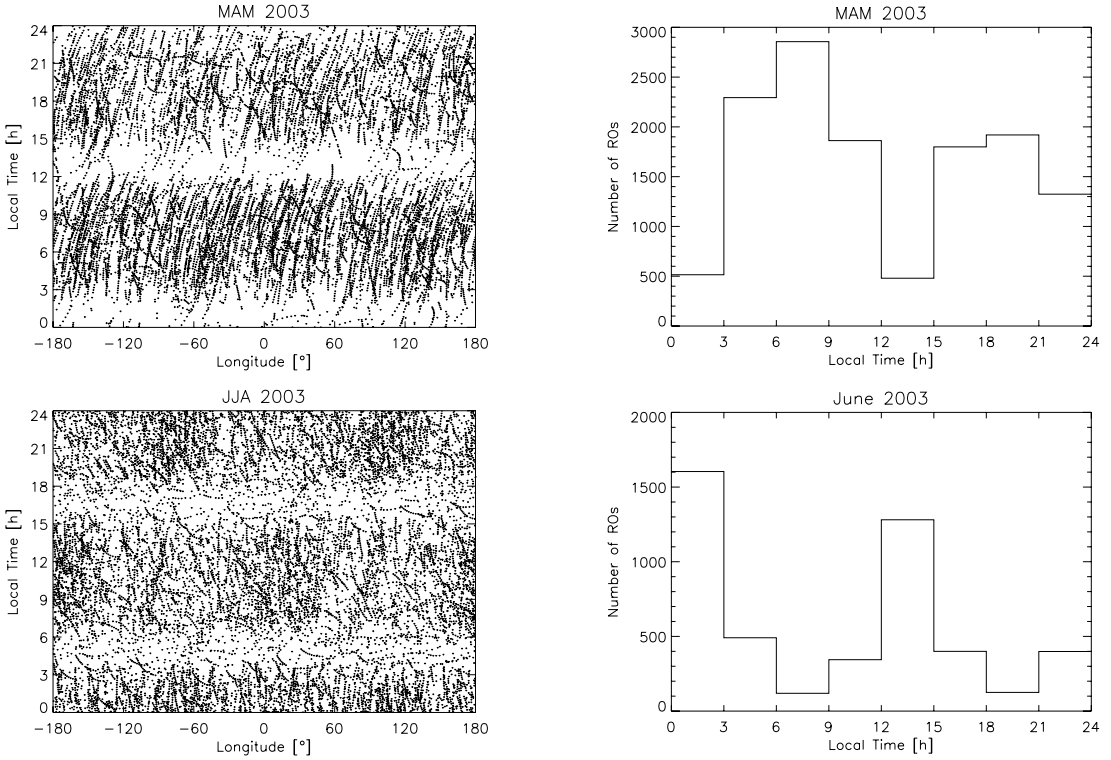

Fig. 6. Local time distribution of CHAMP RO events during two seasons: March, April, May (MAM, top) and June, July, August (JJA, bottom) in 2003. Left: Local time of RO events as a function of longitude. Right: Histogram of number of RO events with three hour time intervals.

Figure 7 shows the local time distribution of CHAMP RO events in a different view – as function of latitude. At latitudes corresponding approximately to the inclination of the CHAMP satellite, the RO events are better distributed in local time due to the approximately zonal orientation of the satellite trajectory.

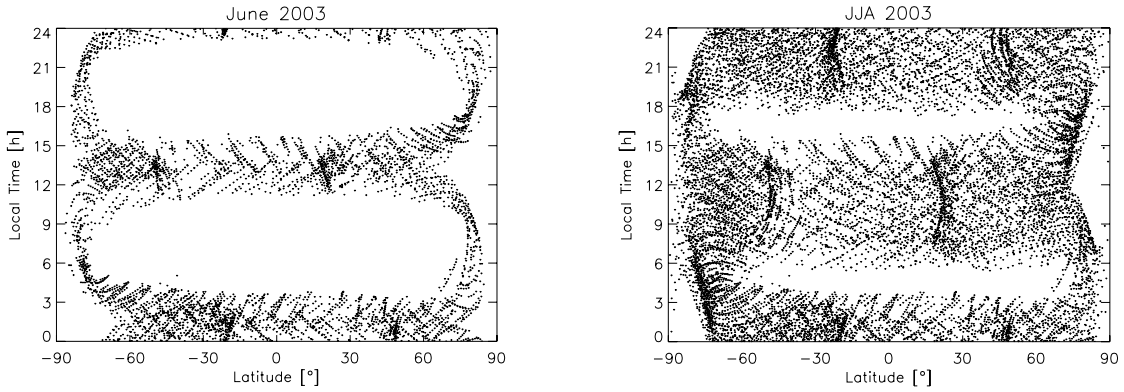

Fig. 7. Local time distribution of CHAMP RO events in June 2003 (left) and JJA 2003 (right) as function of latitude.

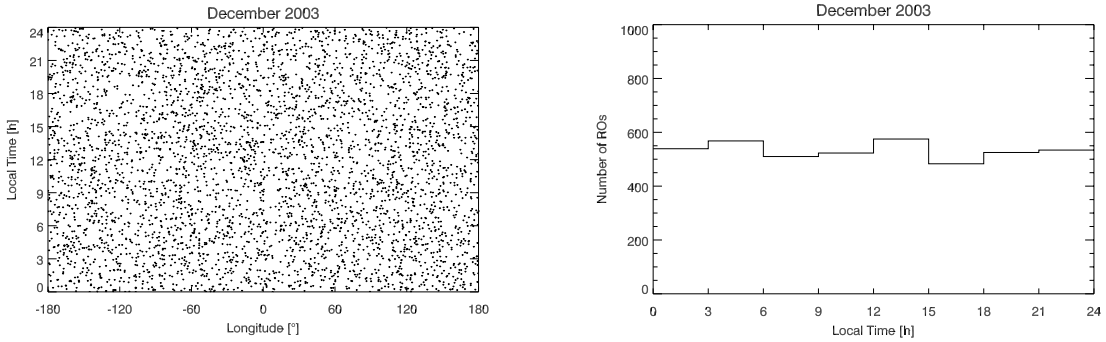

Fig. 8. Distribution of RO events at uniformly randomized time in December 2003. Left: Local time of RO events as a function of longitude. Right: Histogram of the number of RO events with three hour time intervals.

In order to separate the local time influence on the sampling error, we computed dry temperature fields from "true" ECMWF profiles at the RO event locations, but uniformly distributed them in local time. Figure 8 shows this artificial uniform distribution of RO events in time. In order to demonstrate the effect we selected a region and time with an unusually large sampling error (Fig. 9): In December 2003 the cold northern polar vortex is not adequately sampled with CHAMP RO events, resulting in a large positive sampling error in most parts of the domain. The difference plot between the actually occurring and the "artificial" sampling error shows only very small deviations (generally < 0.3 K).

Figure 10 confirms that the large CHAMP sampling error at high northern latitudes is restricted to the month December (2003 and, to a smaller extent, 2002). This provides evidence that the local time contribution to the sampling error is very small even for monthly means under severe sampling conditions (like in December 2003 at high northern latitudes). A separate more complete quantitative study of Local Time effects will be performed in the future.

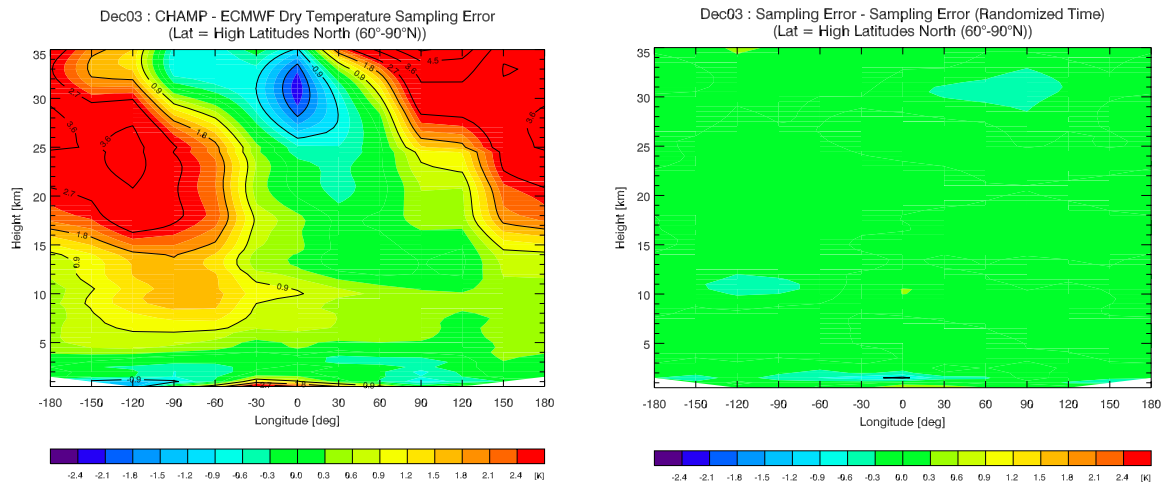

Fig. 9. Left: Sampling error in December 2003 at high northern latitudes computed from RO events in 30° x 30° bins within 60°N and 90°N. Right: Difference between the "true" sampling error and an artificial sampling error computed with profiles at uniformly distributed local times.

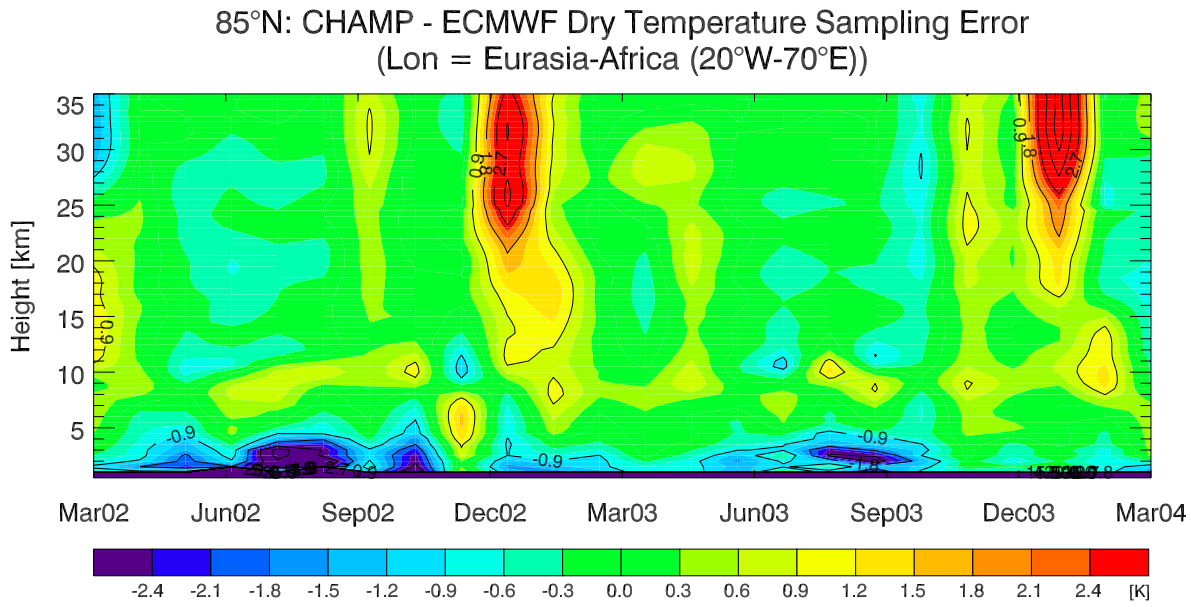

Fig. 10. Sampling error for CHAMP RO dry temperature climatologies from March 2002 to February 2004 at high northern latitudes (80°N to 90°N) in the "Eurasian-African" longitude sector.

4 RO Based Climatologies

The current status of the retrieval and processing system is described in the CHAMPCLIM processing report by *Borsche et al*. (2006b) together with a discussion of the different binning strategies performed within CHAMPCLIM. All results shown in section 4.1 to 4.3 are based on atmospheric profiles obtained with the CCRv2.3 retrieval.

4.1 Error Estimates

4.1.1 Estimation of the Observational Error

We present an estimation of the observational error of the parameters refractivity, pressure, geopotential height, and temperature and simple global models for the observational error based on the analysis of individual profiles.

The estimation of the observational error for these parameters is based on an empirical error analysis study as described in section 3.1 of the CHAMPCLIM processing report (*Borsche et al*., 2006b) and in *Steiner and Kirchengast* (2005) and *Steiner et al.* (2006). In this study we use the global mean of a dataset of two seasons of radio occultation observations DJF 0203 and JJA2003, the data were processed with CCRv2.3 (*Borsche et al*., 2006b). Based on the error statistics of atmospheric difference profiles, i.e., the deviation of CHAMP retrieved profiles from ECMWF co-located profiles ($x_{\mathrm{CHAMP}} - x_{\mathrm{ECMWF}}$), we define the combined error (CHAMP observed error plus ECMWF model error).

For refractivity a separation of these errors was performed by subtracting the estimated ECMWF error from the combined error in terms of variances ($s^2_{\mathrm{obs}} = s^2_{\mathrm{combined}} - s^2_{\mathrm{ECMWF}}$), thus giving an estimate of the observational error. It shows that the estimated ECMWF error and the observational error are approximately of the same order of magnitude. A reasonable and simple estimate of the observed error can thus be given by scaling the combined error with 1/sqrt(2). Especially for pressure and geopotential height, where we do not have estimates of the ECMWF error this seems to be a reasonable approximation.

Based on these observational error estimates, in terms of relative standard deviation (Rel.StdDev) for refractivity and pressure and in terms of absolute standard deviation (StdDev) for geopotential height and temperature, we developed simple global error models. We performed this in fitting simple analytical functions to the Rel.StdDev and StdDev profiles, respectively. We applied a least-squares fit and chose those functional forms with the smallest fit residuum.

The models depend on a few parameters only and exhibit the following simple height dependences. In an upper troposphere/lower stratosphere region the error is closely constant. Above this region it follows an exponential increase with H_{strat} denoting the scale height of the error increase over the stratosphere. Below this region the error is found to increase closely proportional to an inverse height law ("$1/z^p$" law, with $p = 1$ for refractivity and with $p = 0.5$ for pressure, geopotential height and temperature, respectively). In summary, the observation error model $s(z)$ can be formulated as follows:

$$s(z) = \begin{cases} s_{\text{utls}} + s_0\left[(1/z^p) - (1/z_{\text{troptop}}^p)\right], & \text{for } 2\,\text{km} < z \le z_{\text{troptop}} \quad (3a) \\ s_{\text{utls}}, & \text{for } z_{\text{troptop}} < z < z_{\text{stratbot}} \quad (3b) \\ s_{\text{utls}} \cdot \exp\left[(z - z_{\text{stratbot}})/H_{\text{strat}}\right], & \text{for } z_{\text{stratbot}} \le z < 35\,\text{km}. \quad (3c) \end{cases}$$

In Eq. (3a-c) z denotes the altitude, z_{troptop} the top level of the "troposphere domain", z_{stratbot} the bottom level of the "stratosphere domain", s_{utls} the error in the "upper troposphere/lower stratosphere domain", and s_0 the best fit parameter for the "tropospheric" model, respectively (*Steiner and Kirchengast*, 2005; *Steiner et al*., 2006). Using Eq. (3a-c) with the specific values for the respective parameters as listed in Table 1 below, global observation error models can be constructed.

Table 1. Fitting parameters for the observation error models: z_{troptop} denoting the top level of the "troposphere domain", z_{stratbot} the bottom level of the "stratosphere domain", s_{utls} the (Rel.)StdDev between z_{troptop} and z_{stratbot}, s_0 the best-fit parameter for the tropospheric models, p the exponent, and H_{strat} the scale height of error over the lower stratosphere, respectively.

	z_{troptop}	z_{stratbot}	s_{utls}	s_0	p	H_{strat}
Refractivity	14 km	18 km	0.4%	2.5%	1.0	15 km
Pressure	10 km	14 km	0.25%	1.0%	0.5	13 km
Geop.Height	10 km	14 km	15 gpm	60 gpm	0.5	13 km
Temperature	10 km	14 km	0.8 K	5 K	0.5	23 km

Figures 11 to 14 visualize the observational error estimates for refractivity, pressure, geopotential height and temperature, respectively. Displayed are the combined errors (black diamond shaped symbols), the estimated observational errors (combined error/sqrt(2)) (black solid) and the analytical error models (red). In addition we show in Fig. 11 for comparison purposes the estimated observational error for refractivity derived by subtraction of the ECMWF error from the combined error (black dashed).

For its application to climatologies one has to consider the uncertainty of the mean. Thus the estimated observational error (of individual profiles) has to be divided by the square root of the number of occultations ($s(z)$/sqrt[$n_{\text{occ}}(z)$]). For zonal mean seasonal climatologies the number of RO events per bin is typically larger than 400, leading to an error reduction by a factor of at least 20.

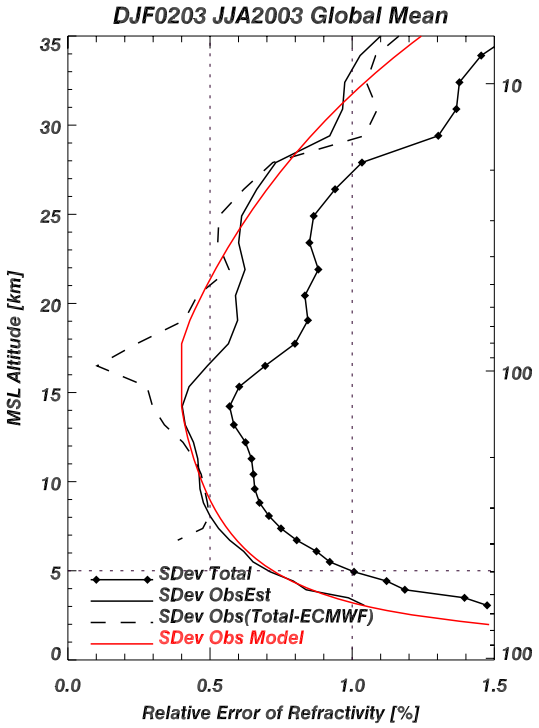

Fig. 11. Rel.StDev of refractivity for the mean of DJF0203 and JJA 2003: combined (black diamond shaped symbols), combined minus ECMWF (black dashed), observed estimated (black solid), model (red).

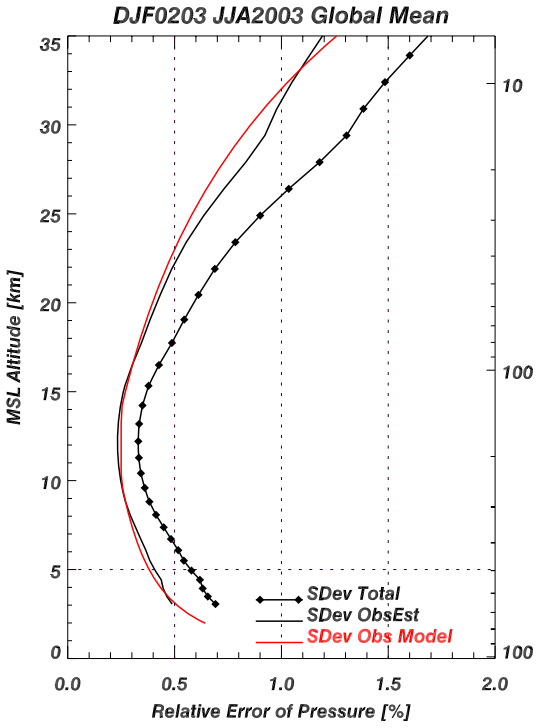

Fig. 12. Rel.StDev of pressure for the mean of DJF0203 and JJA 2003: combined (black diamond shaped symbols), observed estimated (black solid), model (red).

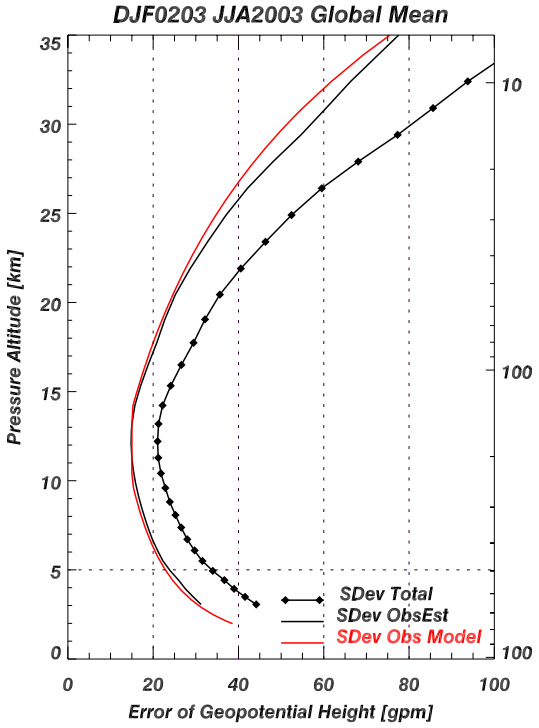

Fig. 13. StDev of geopotential height for the mean of DJF0203 and JJA 2003: combined (black diamond shaped symbols), observed estimated (black solid), model (red).

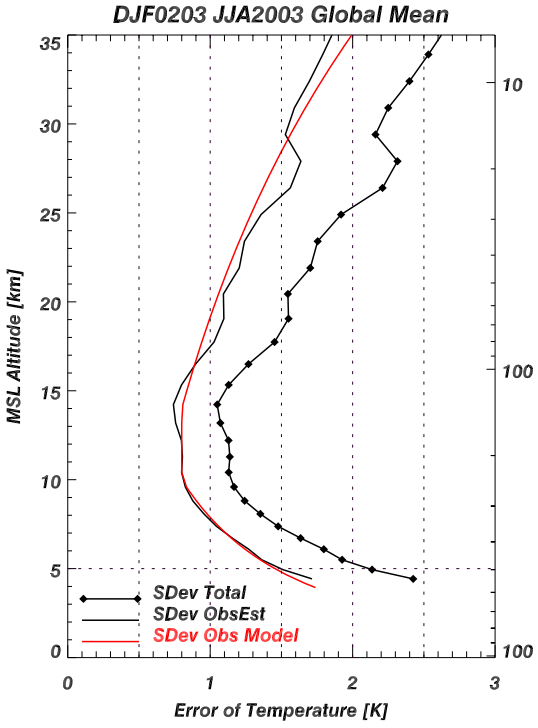

Fig. 14. StDev of temperature for the mean of DJF0203 and JJA 2003: combined (black diamond shaped symbols), observed estimated (black solid), model (red).

As a first step the presented error models provide a reasonable estimate of the global observational error for CHAMP profiles of refractivity, pressure, geopotential height and temperature. As a next step further advancement of the global error models is foreseen with respect to an extension including the latitudinal and seasonal variation of the observation error. This aspect becomes important at upper stratospheric altitudes especially at high latitudes where a larger error in winter than in summer is revealed (compare Figures 17 to 21, section 3.1 of the CHAMPCLIM processing report (*Borsche et al*., 2006b)).

The winter/summer variation at stratospheric altitudes can be well captured through sinusoidal seasonal variation of the stratospheric error scale height H_{strat}, with larger values of H_{strat} giving a smaller error and vice versa. Variations of the error at lower tropospheric heights can likewise be modeled by a variation of the parameter s_0, with a smaller value of s_0 giving a smaller error and a larger value of s_0 leading to a larger error in this height region.

The described extensions of the global models are foreseen to be analyzed and implemented in the near future. Thus, these simple analytical models with a few adjustment parameters only will be able to capture the observational error with its seasonal and latitudinal dependence. The inclusion of the number of occultation events will provide the observational error for refractivity, pressure, geopotential height, and temperature climatologies.

4.1.2 Estimation of the Sampling Error

Based on the results of the sampling error study (see section 2) we developed a strategy for the provision of sampling error estimates. The complex temporal evolution of the sampling error prohibits a simple formulation as in the case of observational errors (section 4.1.1). We will therefore provide an estimated corresponding sampling error field to every atmospheric climatology field.

Section 4.2 includes a host of examples for such sampling error fields for a complete set of seasonal temperature climatologies over four years (Dec 2001 – Nov 2005).

4.2 Seasonal CHAMP Temperature Climatologies

For the results shown here, we sampled CHAMP dry temperature profiles in 18 latitude bands (10° latitudinal extent). Figure 15 displays the different CHAMPCLIM products for the "testbed" season JJA 2003.

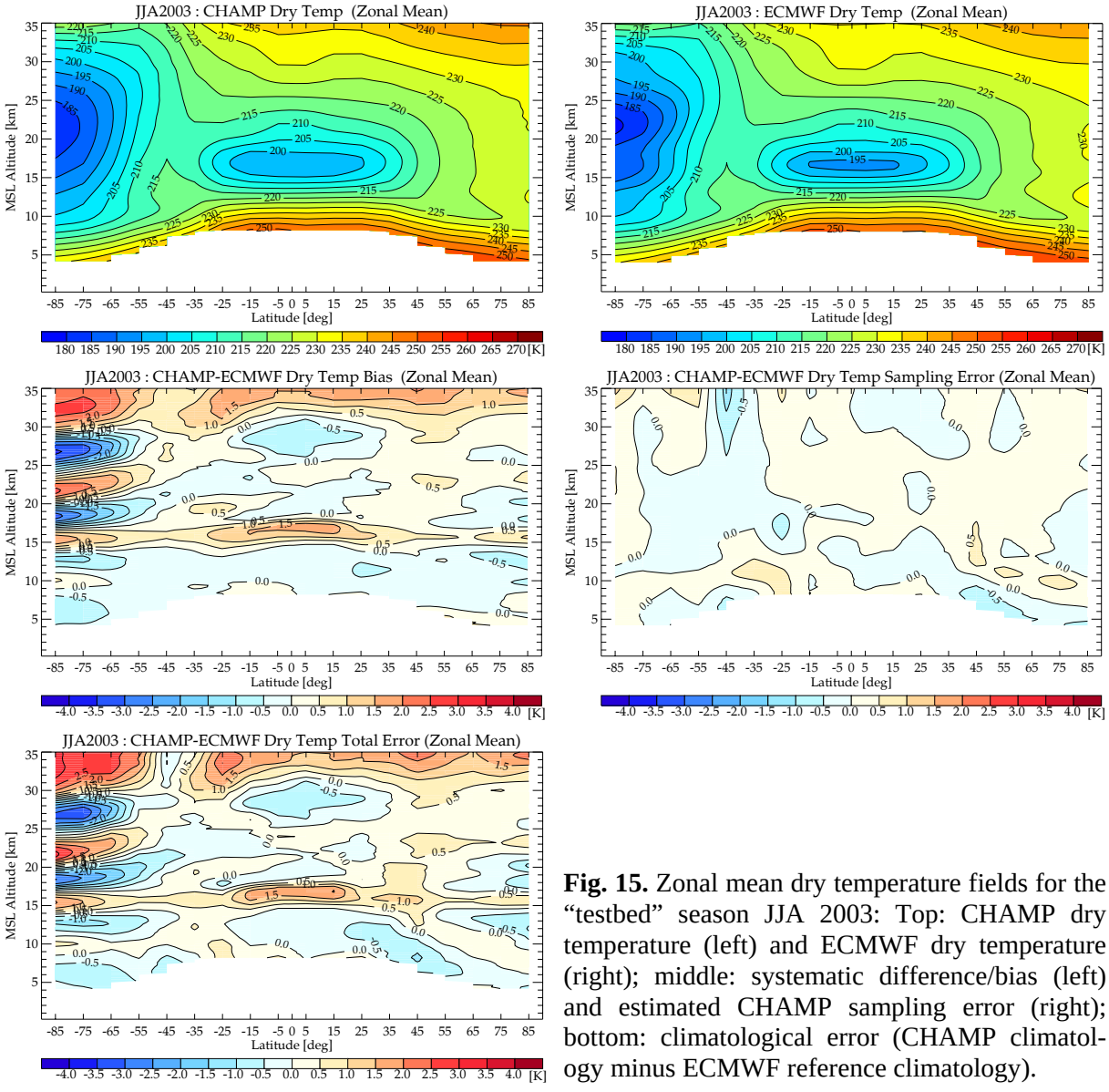

Fig. 15. Zonal mean dry temperature fields for the "testbed" season JJA 2003: Top: CHAMP dry temperature (left) and ECMWF dry temperature (right); middle: systematic difference/bias (left) and estimated CHAMP sampling error (right); bottom: climatological error (CHAMP climatology minus ECMWF reference climatology).

Latitudinally and vertically resolved difference statistics have been computed by comparing each CHAMP RO profile with a co-located ECMWF analysis profile. The systematic difference for the (northern) summer season (JJA 2003) is shown in the middle left panel of Fig. 15 (taking ECMWF as reference).

The differences above 30 km are most probably due to errors in both CHAMP and ECMWF. In the height range, where RO data have the highest quality (~8 km to ~30 km), the

agreement between CHAMP and ECMWF is, in general, very good: The absolute bias is < 0.5 K, occasionally peaking at 1 K. However, two features are prominent:

The tropical tropopause region in the CHAMP-derived fields is consistently warmer than the ECMWF analyses. This difference is probably caused by a weak representation of atmospheric wave activity and tropopause height variability in ECMWF fields, but work is ongoing to explain the discrepancies in detail (see also section 4.4.1).

The wave-like bias structure with a magnitude of several degrees in the southern winter polar vortex region (JJA 2003) is caused by deficiencies in the representation of the austral polar vortex in the ECMWF analyses. A detailed analysis can be found in *Gobiet et al.* (2005b) and in *Foelsche et al.* (2006).

The climatological error in the UTLS region is therefore not only caused by errors in CHAMP RO data but contains also considerable errors of the reference dataset (ECMWF).

Seasonal zonal-mean dry temperature fields from CHAMP and ECMWF, respectively, for DJF 2001/2002 to SON 2005 are shown in Figs. 16, 18, 20, and 22. The corresponding systematic differences and CHAMP sampling errors are displayed in Figs. 17, 19, 21, and 23, respectively.

The continuous data stream of CHAMP RO data started in March 2002; during the winter season DJF 2001/2002 the amount of available RO profiles was considerably smaller, but still sufficient to build climatologies, at least on a zonal mean basis. Altogether the climatology thus covers a period of four complete years from Dec 2001 to Nov 2005.

The systematic difference in the tropical tropopause region (CHAMP warmer than ECMWF) is a persistent feature in all seasons under consideration. The wave-like bias structure in the austral polar vortex region can be seen in all (northern) summer seasons. In JJA 2002, a year with a weak polar vortex, it is less pronounced. During JJA 2004 this bias structure is again less pronounced, probably due to the addition of new data to the ECMWF analysis scheme in October 2003 (AIRS radiances) and changes in the assimilation scheme like bias adjustments of satellite data (A. Simmons, ECMWF, pers. communication, 2005). In JJA 2005, however, the bias structure is even stronger than before. Interestingly, the phase has changed the sign.

The CHAMP sampling errors during summer and winter are generally small, only occasionally exceeding 0.5 K. During fall, especially SON 2003 and 2004, there is considerable sampling error at southern (and northern) high latitudes. A similar but less distinct feature can be observed during spring. These occasional sampling error increases can be explained by clustering of RO events and uneven sampling of the polar vortices (see section 3.2).

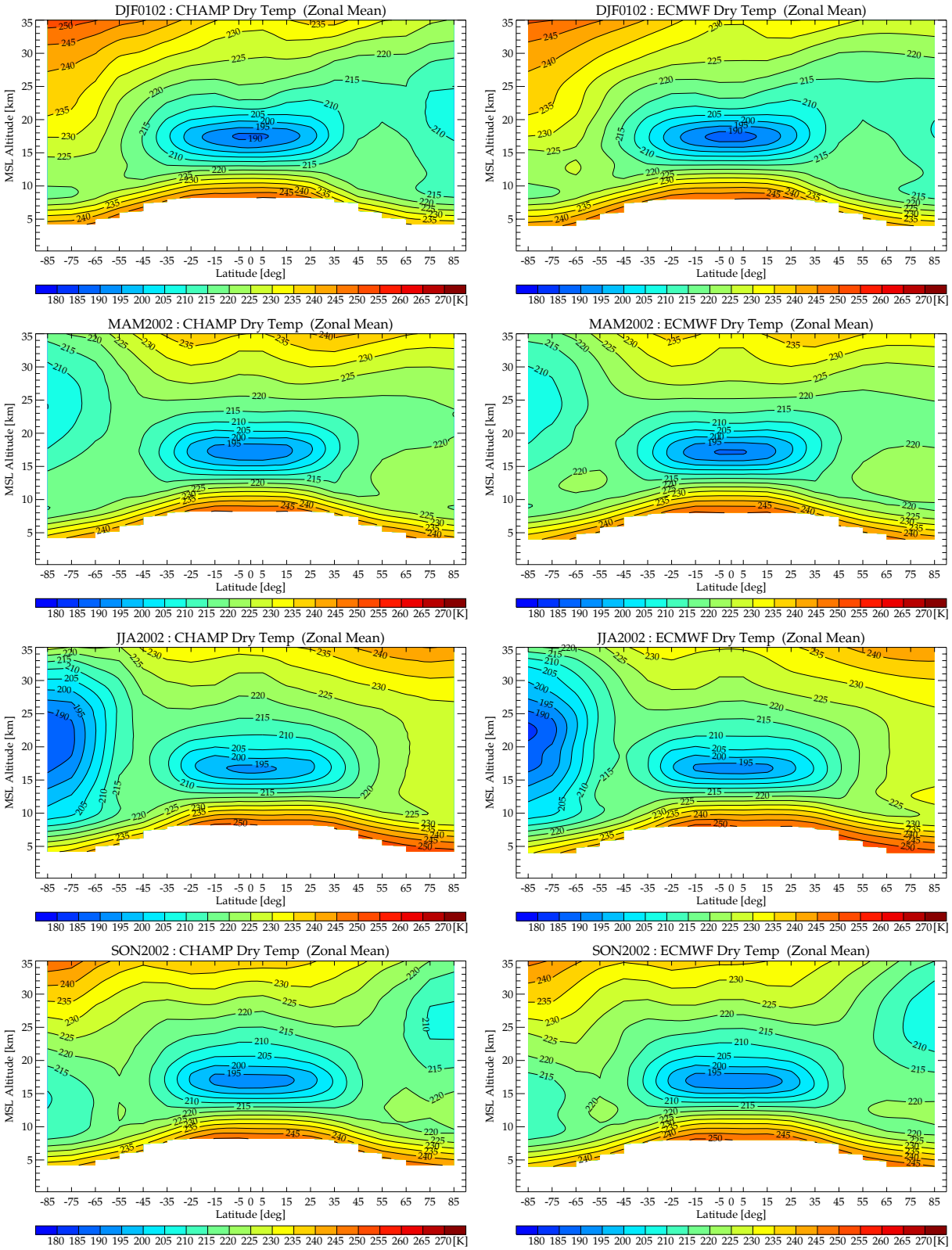

Fig. 16. Zonal mean dry temperature fields for the seasons DJF 2001/2002, MAM 2002, JJA 2002, and SON 2002 (from top to bottom): Retrieved CHAMP fields (left) and ECMWF reference fields (right).

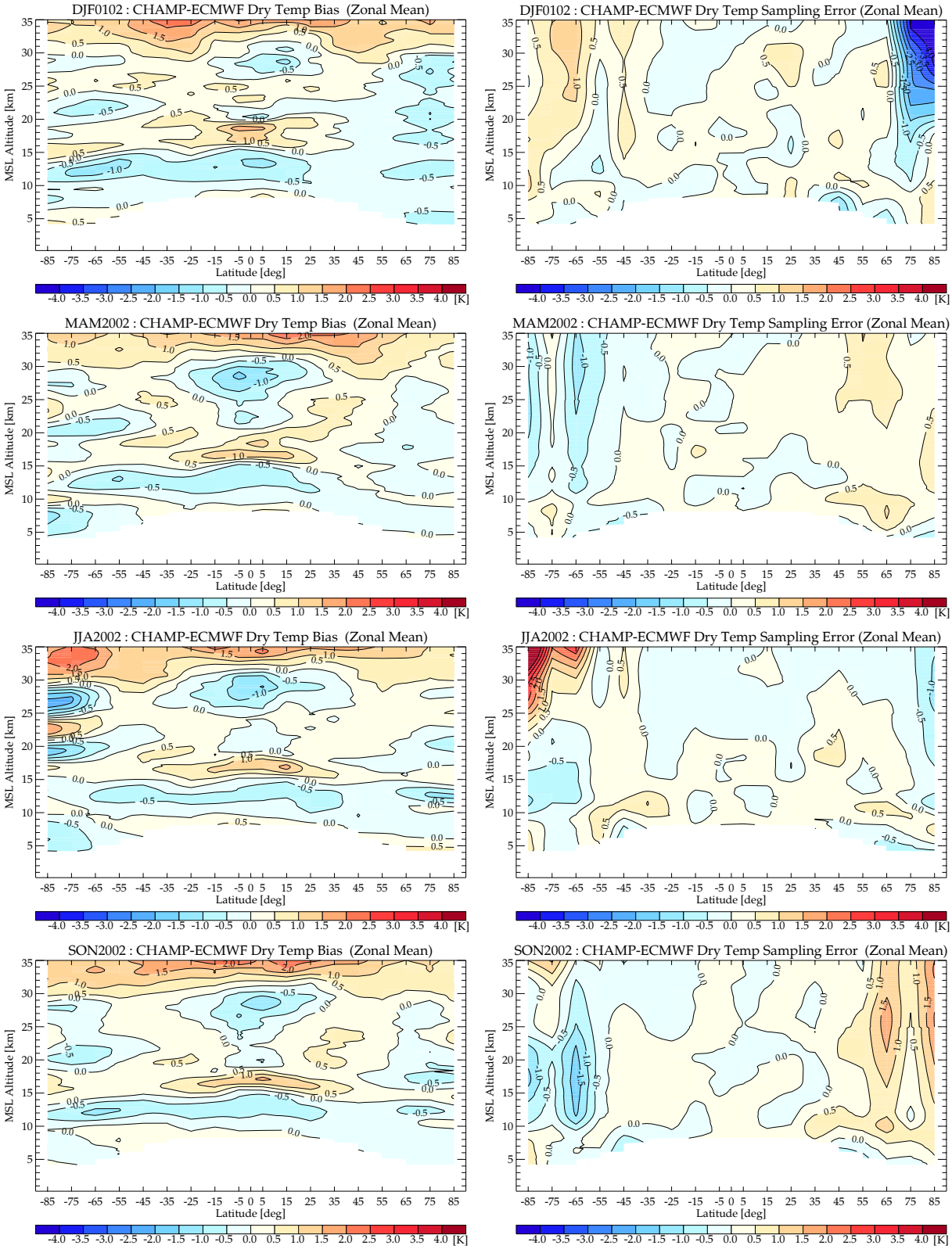

Fig. 17. Zonal mean fields for the seasons DJF 2001/2002, MAM 2002, JJA 2002, and SON 2002 (from top to bottom): Systematic difference/bias between CHAMP and ECMWF (left) and CHAMP sampling error (right).

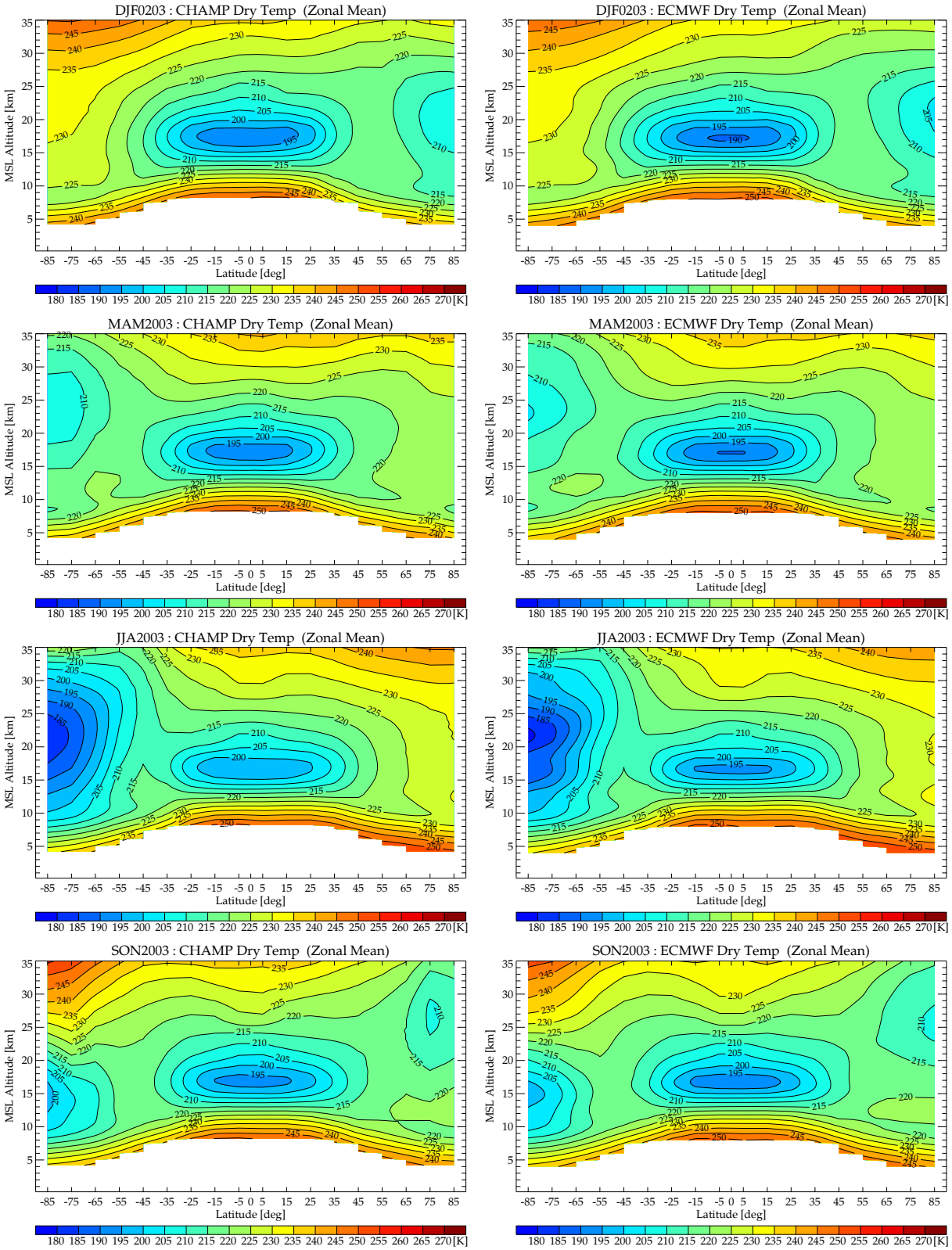

Fig. 18. Zonal mean dry temperature fields for the seasons DJF 2002/2003, MAM 2003, JJA 2003, and SON 2003 (from top to bottom): Retrieved CHAMP fields (left) and ECMWF reference fields (right).

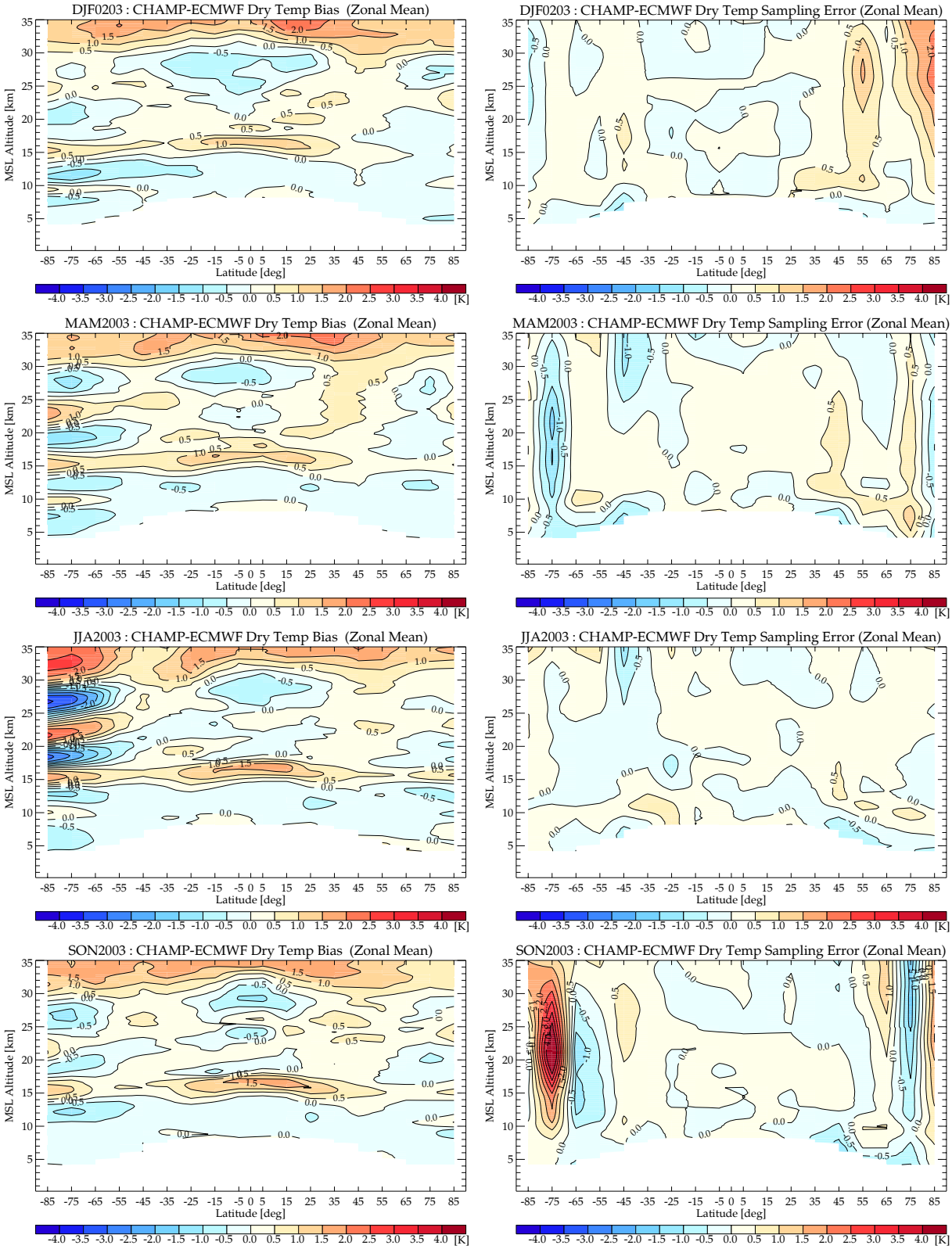

Fig. 19. Zonal mean fields for the seasons DJF 2002/2003, MAM 2003, JJA 2003, and SON 2003 (from top to bottom): Systematic difference/bias between CHAMP and ECMWF (left) and CHAMP sampling error (right).

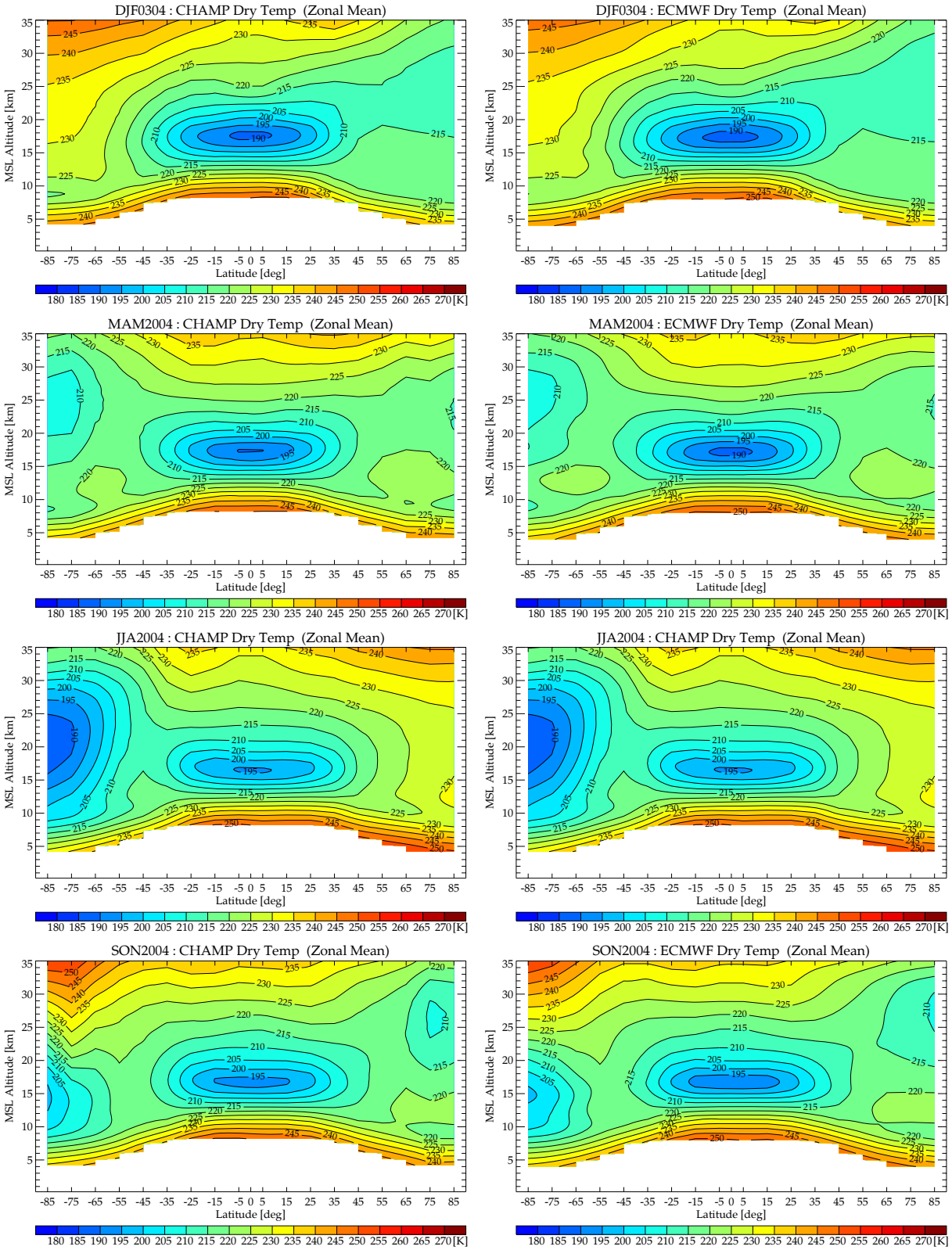

Fig. 20. Zonal mean dry temperature fields for the seasons DJF 2003/2004, MAM 2004, JJA 2004, and SON 2004 (from top to bottom): Retrieved CHAMP fields (left) and ECMWF reference fields (right).

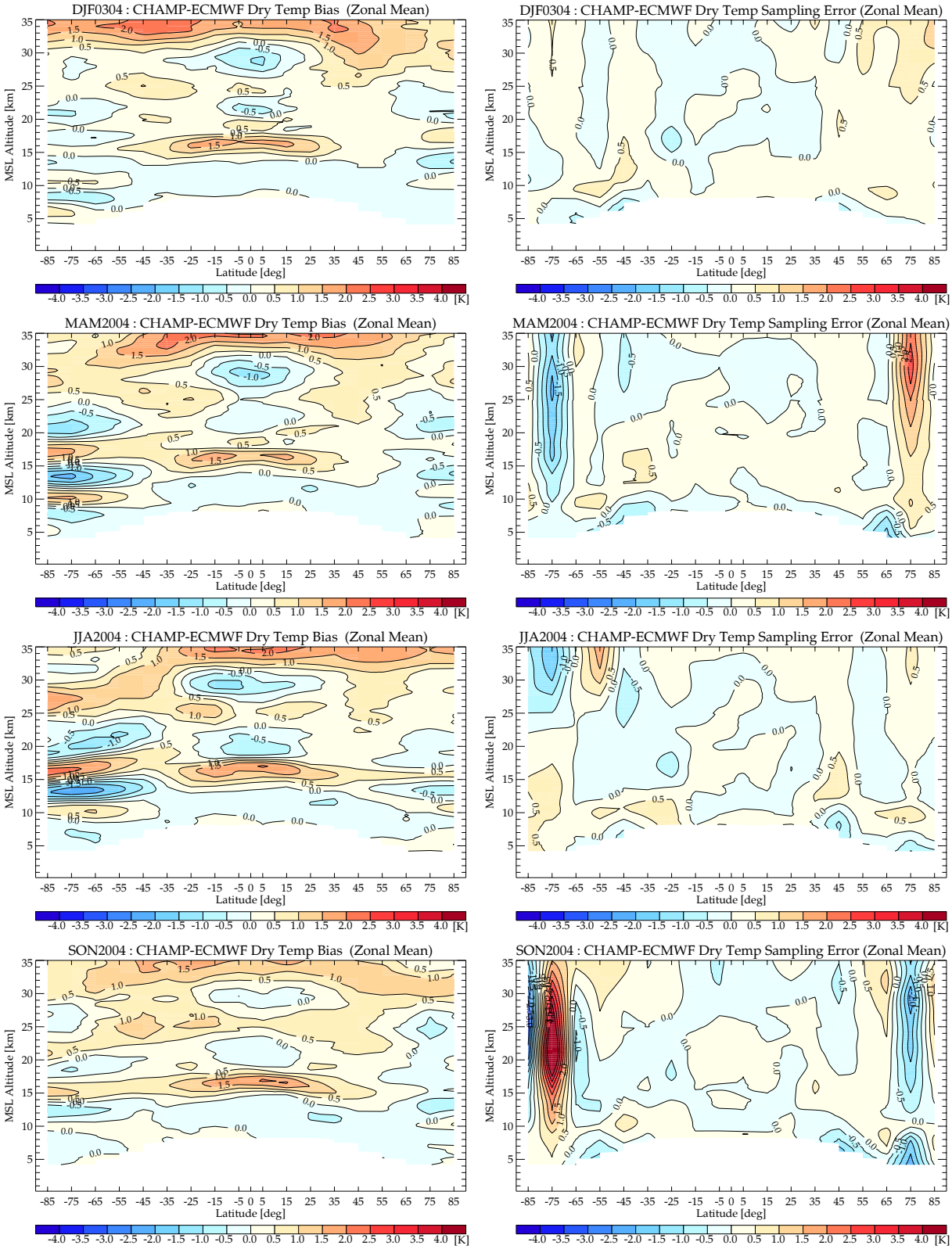

Fig. 21. Zonal mean fields for the seasons DJF 2003/2004, MAM 2004, JJA 2004, and SON 2004 (from top to bottom): Systematic difference/bias between CHAMP and ECMWF (left) and CHAMP sampling error (right).

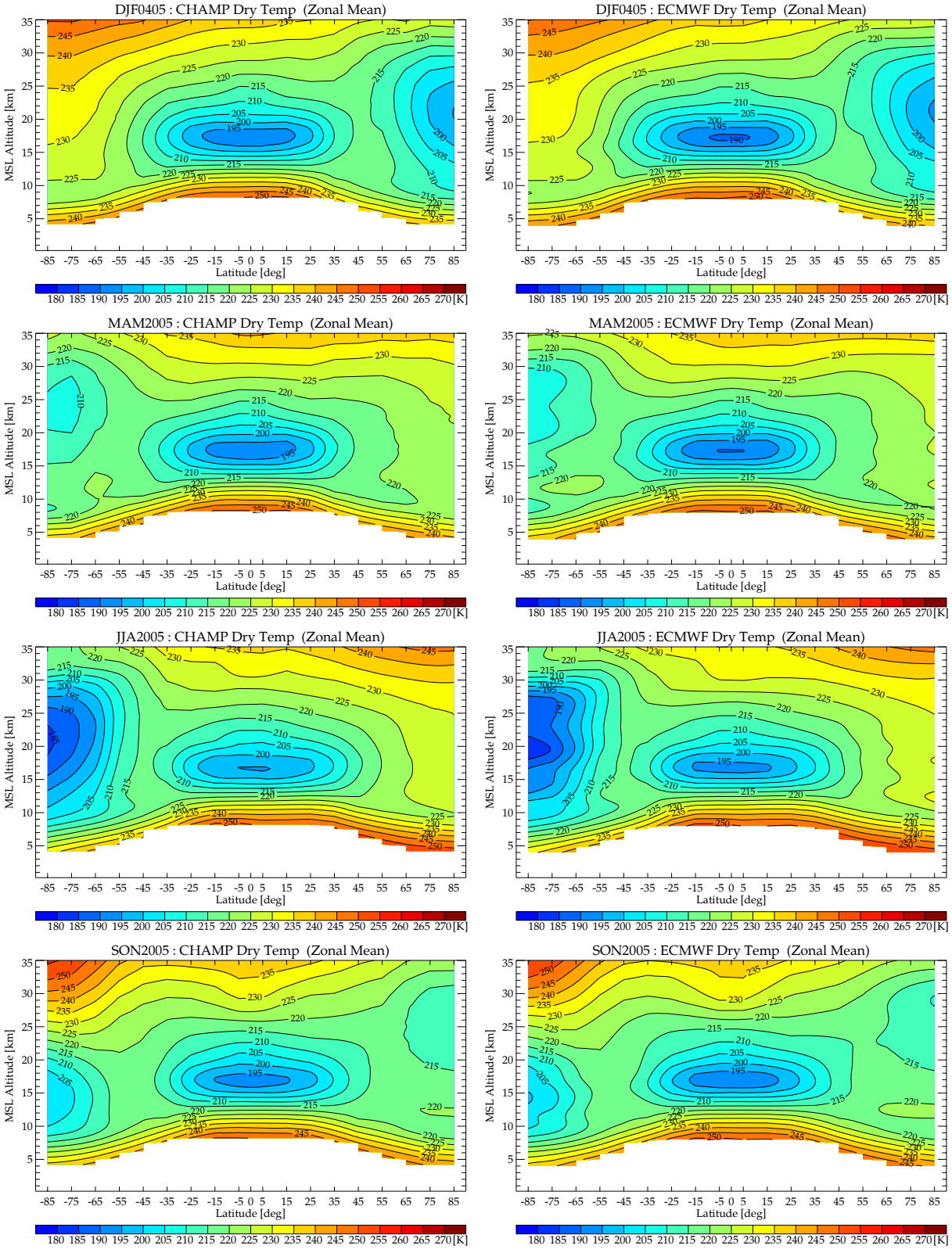

Fig. 22. Zonal mean dry temperature fields for the seasons DJF 2004/2005, MAM 2005, JJA 2005, and SON 2005 (from top to bottom): Retrieved CHAMP fields (left) and ECMWF reference fields (right).

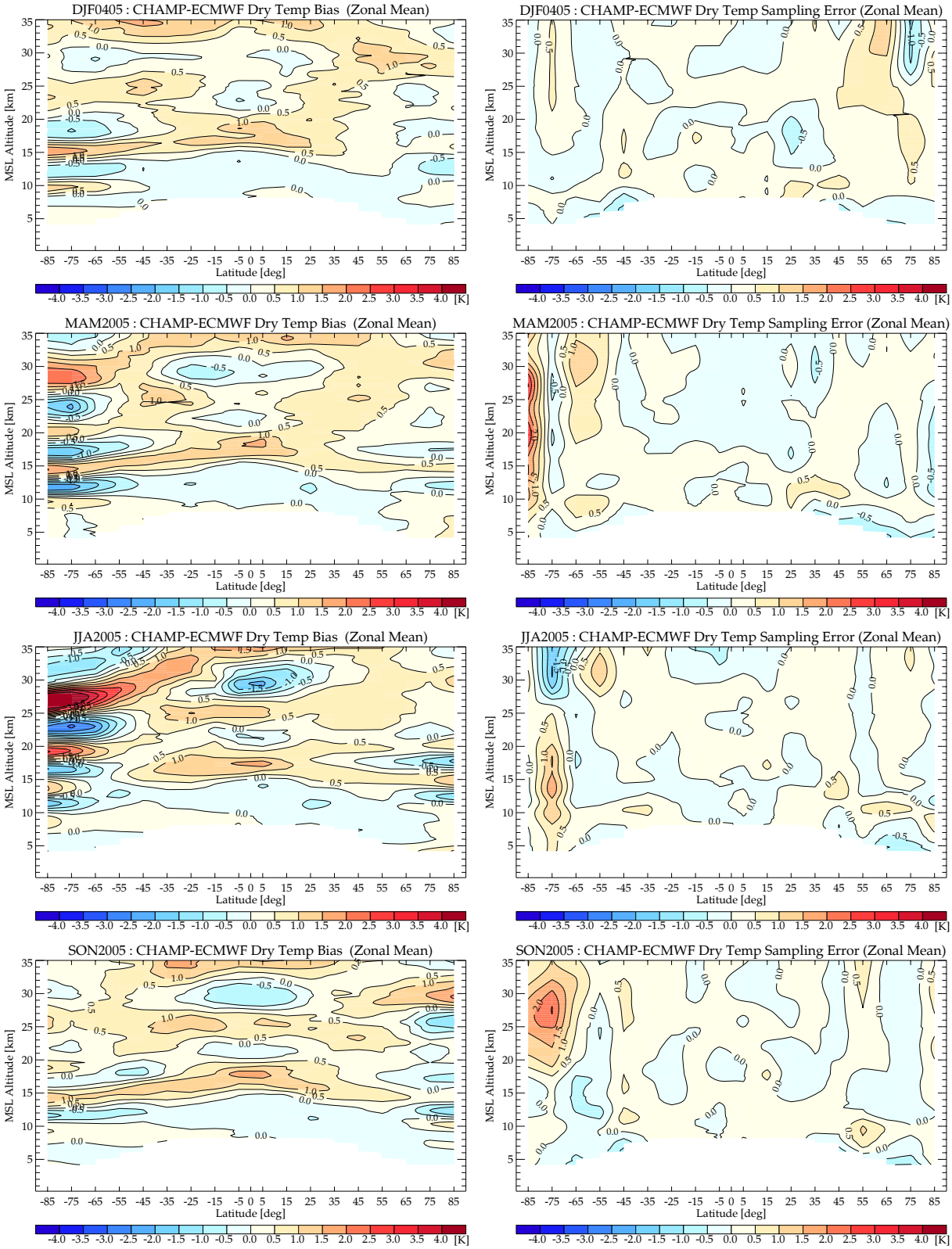

Fig. 23. Zonal mean fields for the seasons DJF 2004/2005, MAM 2005, JJA 2005, and SON 2005 (from top to bottom): Systematic difference/bias between CHAMP and ECMWF (left) and CHAMP sampling error (right).

4.3 CHAMPCLIM Multi-Parameter Fields

Within CHAMPCLIM we started building climatologies of the atmospheric parameters refractivity, pressure, and geopotential height as well. Refractivity fields for DJF 2002/2003 and JJA 2003 with the corresponding errors are displayed in Fig. 24. The relative refractivity bias in JJA 2003 mirrors the corresponding (absolute) dry temperature difference, with negative deviations where the temperature deviations are positive and vice versa.

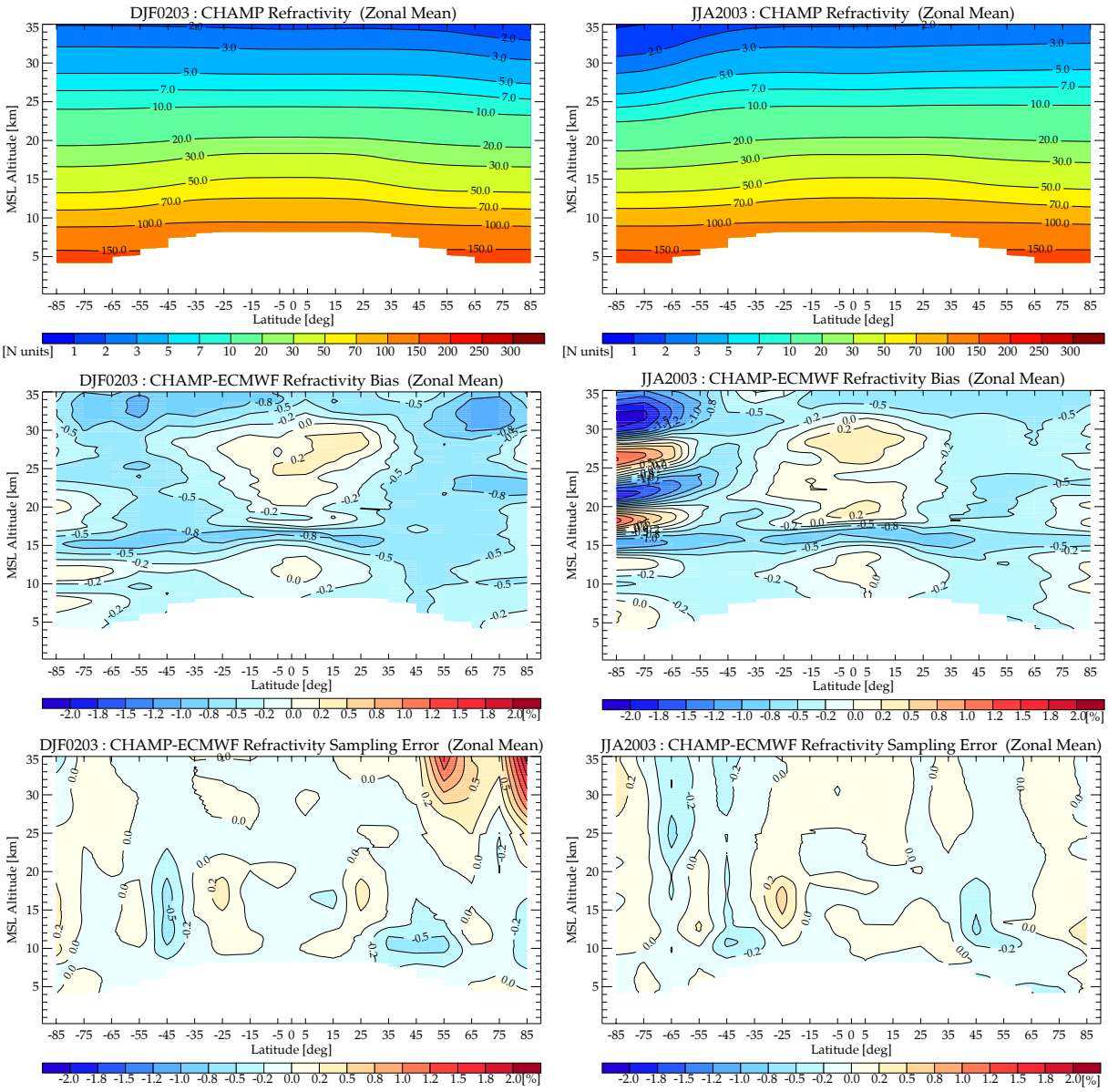

Fig. 24. Zonal mean fields for the seasons DJF 2002/2003 (left) and JJA 2003 (right): Top: CHAMP refractivity climatologies, middle: systematic (relative) difference/bias between CHAMP and ECMWF, bottom: relative CHAMP sampling error.

Pressure fields for DJF 2002/2003 and JJA 2003 with the corresponding errors are displayed in Fig. 25. The selected pressure contour levels in the top panels of Fig. 25 reflect the "mandatory pressure levels" of radiosonde observations.

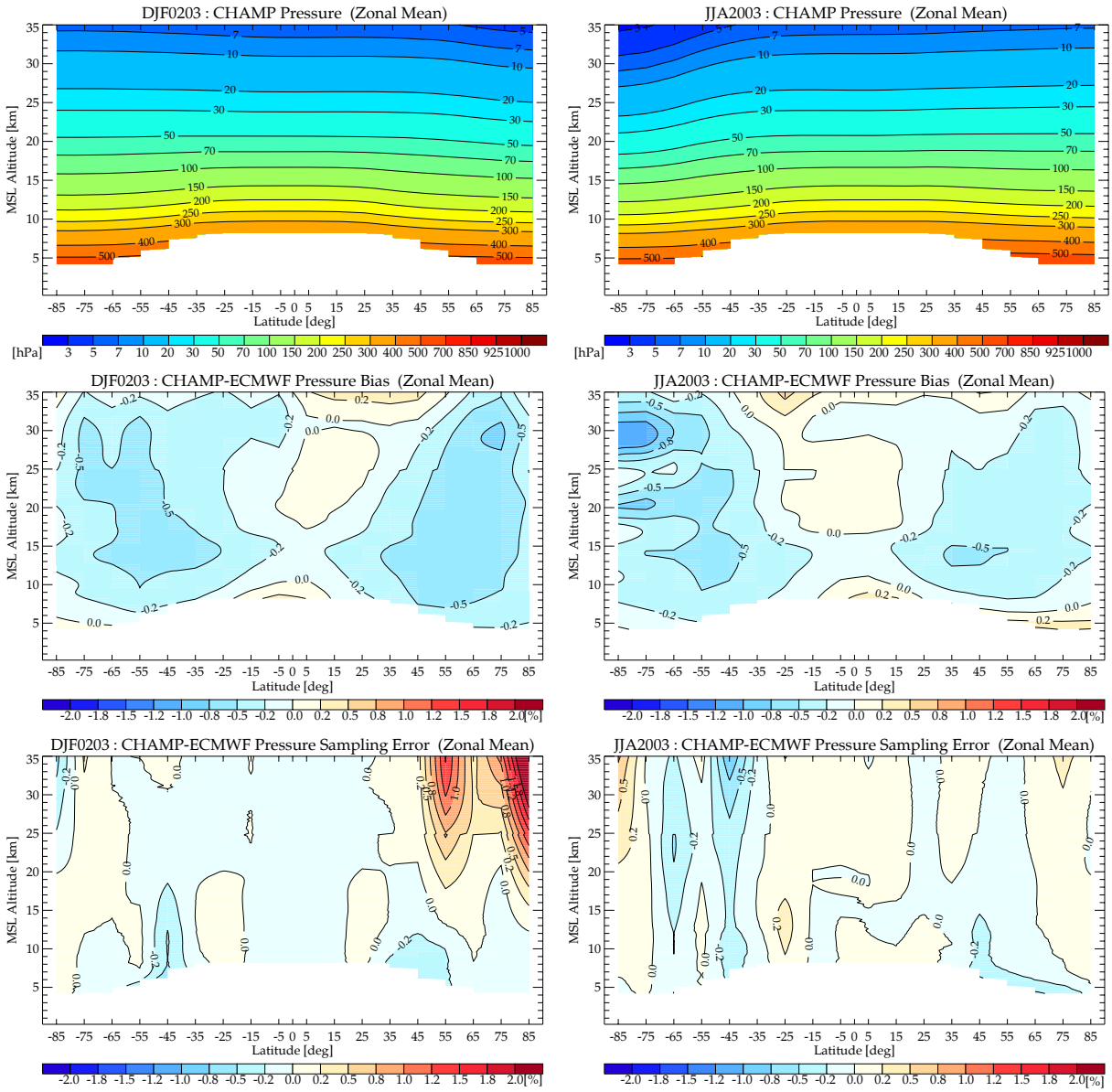

Fig. 25. Zonal mean fields for the seasons DJF 2002/2003 (left) and JJA 2003 (right): Top: CHAMP pressure climatologies, middle: systematic (relative) difference between CHAMP and ECMWF, bottom: relative CHAMP sampling error.

Geopotential height fields for DJF 2002/2003 and JJA 2003 with corresponding errors are displayed in Fig. 26 as function of pressure altitude z_p. The pressure altitude, defined as $z_p[\text{km}] = -7 \cdot \ln(p[\text{hPa}]/1013.25)$, is closely aligned with geometrical altitude z. We note that (absolute) geopotential height errors mirror (relative) pressure errors.

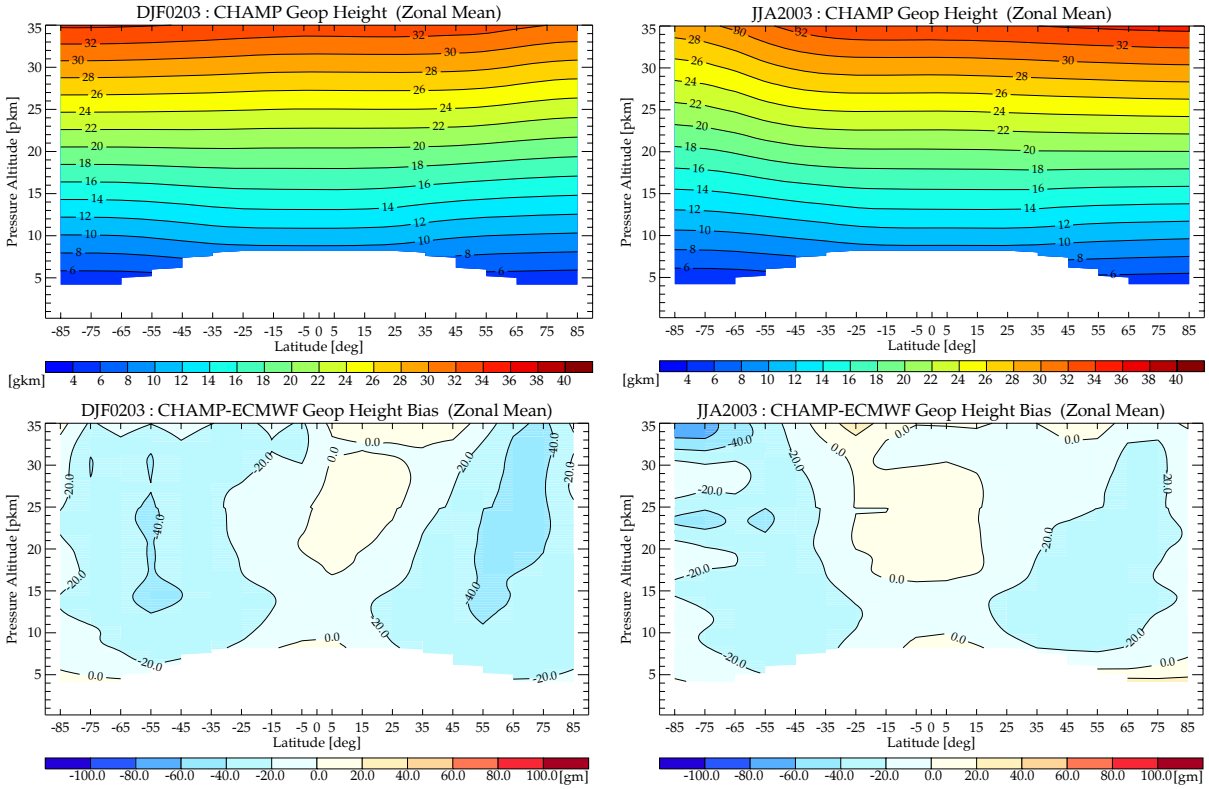

Fig. 26. Zonal mean fields for the seasons DJF 2002/2003 (left) and JJA 2003 (right): Top: CHAMP geopotential height climatologies, bottom: systematic difference between CHAMP and ECMWF.

4.4 Special CHAMPCLIM Products

4.4.1 Tropopause Parameters

The current version of the retrieval, CHAMPCLIM Retrieval version 2.3 (CCRv2.3), has implemented several new features compared to the previous version as described in *Gobiet et al*. (2004). An important enhancement is the calculation of tropopause parameters such as lapse rate tropopause height and temperature and cold point tropopause height and temperature. A detailed discussion can be found in the CHAMPCLIM processing report by *Borsche et al*. (2006b).

The lapse rate tropopause is calculated according to the definition of the World Meteorological Organization (WMO). Here, the tropopause is defined as the lowest level at which the temperature lapse rate is less than 2 K/km and the lapse rate average between this level and the next two kilometers does not exceed 2 K/km (*WMO*, 1957). In the low latitude region (±30°) the lapse rate tropopause is clearly defined with the criterion from WMO.

The cold point tropopause is defined as the coldest point of the profile in the upper troposphere and lower stratosphere region (5 km – 35 km).

Seasonal changes of the height of the tropopause over four years are shown in Fig. 27, the corresponding temperature changes in Fig. 28. CHAMP data resolve and display more variability and cold point tropopause heights are consistently higher than in ECMWF. More detailed comparison of tropical tropopause characteristics will be performed in the future.

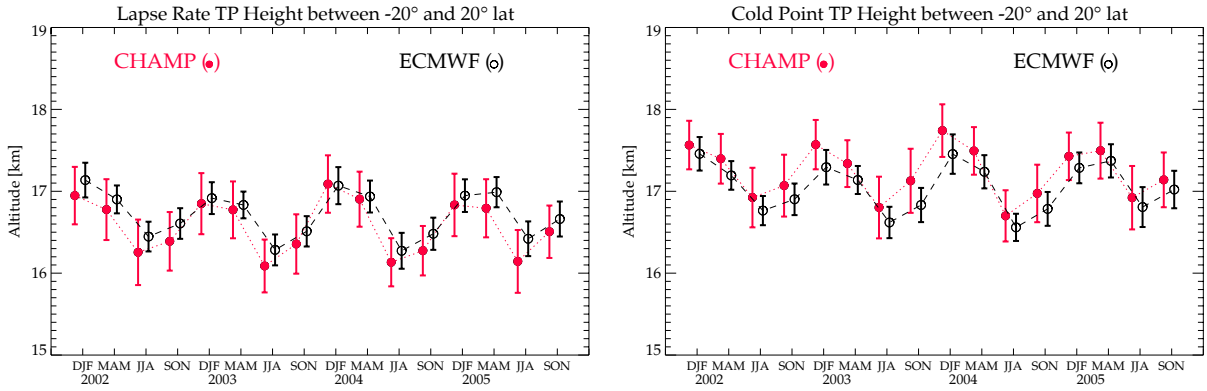

Fig. 27. Lapse rate (left) and cold point tropopause height (right) as zonal and seasonal means between 20°N and 20°S from DJF 2001/02 to SON 2005 ("Error bars": standard deviation of tropopause height variability of individual profiles about the climatological mean height).

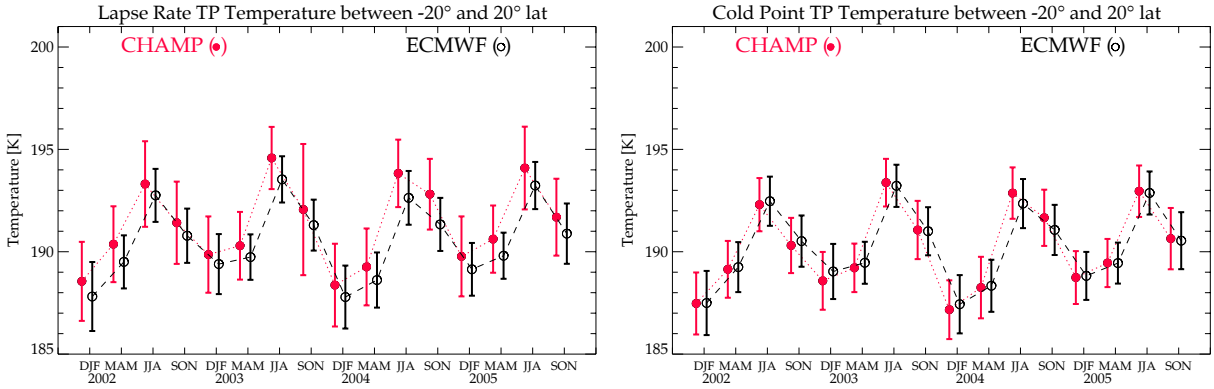

Fig. 28. Lapse rate (left) and cold point tropopause temperature (right) as zonal and seasonal means between 20°N and 20°S from DJF 2001/02 to SON 2005 ("Error bars": standard deviation of tropopause temperature variability of individual profiles about the climatological mean temperature).

4.4.2 Principal Component Analysis (PCA)

The gridded CHAMPCLIM climatology datasets allow for advanced statistical analyses. As an example we show exemplary results of a principal component analysis (PCA) based on CHAMPCLIM climatologies. A detailed description can be found in *Lackner and Pirscher* (2005).

The PCA belongs to the large family of methods for multivariate (statistical) analysis. General information about multivariate data analysis can be found in *Reyment and Jöreskog* (1993), a detailed description of the PCA can be found in *Jolliffe et al.* (2002).

Depending on the purpose of a study and the disciplines, multivariate statistical analysis techniques have two main applications:

The first one is the reduction of data. To reduce a large number of variables to a smaller number of "factors" for modeling purposes is the most common application. The second one is the detection of an underlying structure in the data. The PCA tries to unveil patterns of relationship among many dependent variables.

The mathematical technique used in PCA is called eigenanalysis. It transforms a set of p variables linearly and orthogonally into a number of new hypothetical variates, called principal components (PCs), which are uncorrelated. To define these new variables, the eigenvalues (arranged in descending order) and respective eigenvectors of a covariance or correlation matrix are used. The new variables are chosen in a way that the first variable accounts for the maximum variance of the data, the second for the maximum residual variance and so on. In most cases, few new variables explain a large proportion of the total variance found in the data, and cumulatively, all the new variables account for 100 % of the intrinsic variation.

If the data field is composed of atmospheric data, which are arranged in grid points at different times, the results of a principal component analysis are the PCs representing the temporal evolution of the data and the coefficients depicting their spatial distribution. To make a correct interpretation of the results, it is necessary to consider both PCs and coefficients because they are based on the decomposition of matrices in eigenvectors and it has to be kept in mind that the direction of the eigenvectors is arbitrarily defined.

As an example, two results of a principal component analysis (calculated by means of the correlation matrix) applied to CHAMP RO data are shown. Both times dry temperature data are analyzed, which were used between March 2002 and February 2005, yielding a 36 months observation period. The example data used are drawn from high southern latitudes and from low latitudes, respectively.

The dry temperature data in the south polar region are given as a zonal mean temperature field with a 5° latitudinal resolution (5° bands from 57.5°S to 87.5°S), yielding 6 zonal bands, and a vertical resolution of 5 km (7 height levels from 5 to 35 km). The data are centered to the 3-years mean value at each grid point, so the seasonal cycle is remained in the data.

The second analyzed field is located at low latitudes between 17.5°S and 17.5°N (zonal-mean 5° bands yielding 7 latitudinal regions) to investigate the tropical atmosphere between 12 km and 22 km (vertical resolution: 2 km, yielding 6 vertical layers). Generally, the seasonal fluctuations are less pronounced at low latitudes compared to high latitude regions. Hence the results of PCA will be calculated in this case from data centered each month separately to the 3-year monthly mean at each grid point, eliminating the seasonal cycle.

High Southern Latitudes

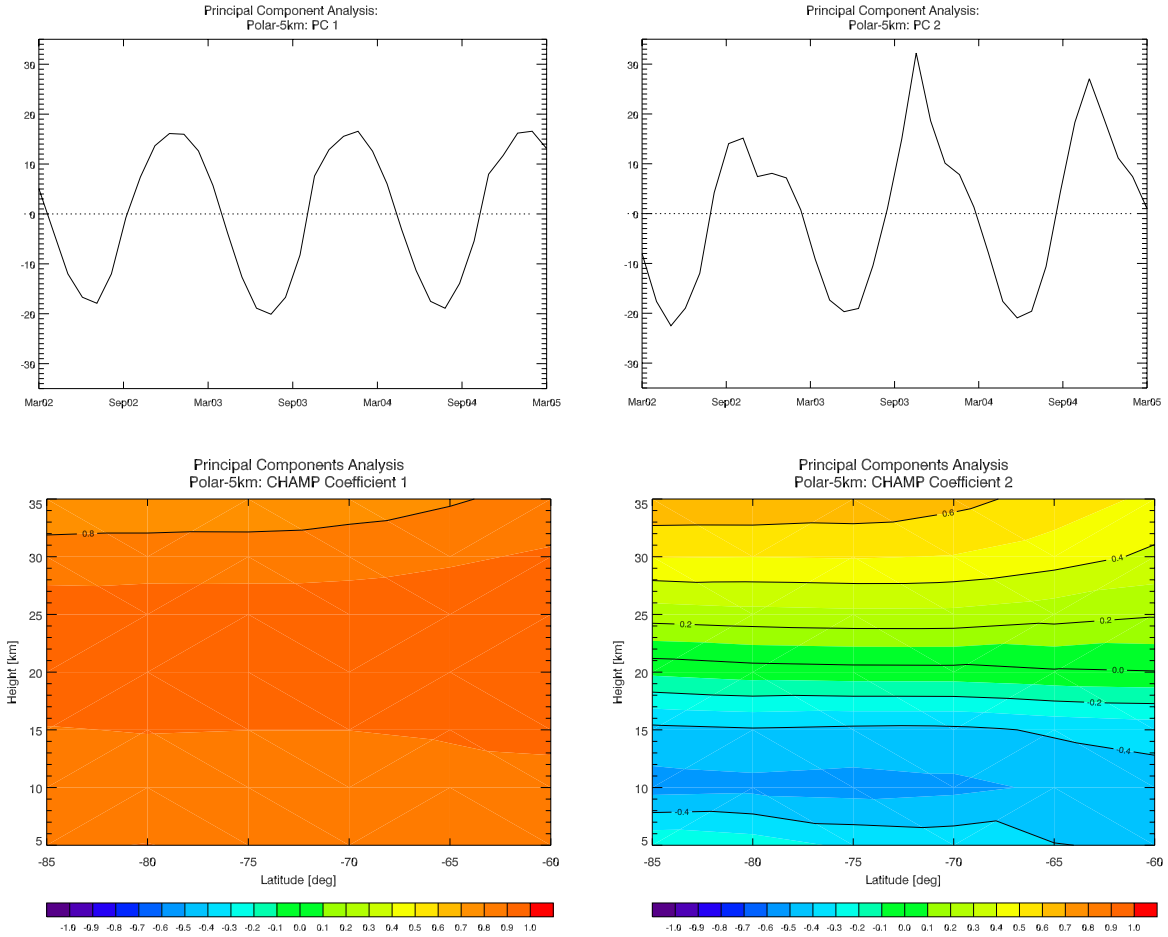

Fig. 29. First and second principal component (top) and corresponding coefficients (bottom) calculated by means of the correlation matrix from the south polar dataset.

The sinusoidal curve of the first principal component, depicted in Fig. 29 (top left), clearly reflects the seasonal cycle. The maximum temperature anomaly arises in December and January each year, lowest values can be found in July and August.

The structure arising in the first coefficient (Fig. 29 bottom left) is homogeneous across all latitudes and all heights. The first PC and its corresponding coefficient account for 78.7% of the intrinsic variation.

The second principal component, depicted in Fig. 29 (top right), also shows the seasonal cycle with the phase being shifted compared to the temporal variation of the first PC. The maxima emerge in October and November, minima occur in June and July.

The respective coefficient (Fig. 29 bottom right) shows a height dependent pattern, altitudes above 21 km display an inverted structure to heights below 21 km. The second PC and its coefficient account for 17.4% of the total variance, so more than 95% of the total variance can be explained by the first two PCs/coefficients.

The reconstruction of the data by means of the first and the second PCs/coefficients, shown in Figure 30, reproduces the seasonal cycle very well. The reconstructed fraction of the second factor is primarily responsible for the earlier temporal warming and cooling of the higher altitudes compared to near surface regions.

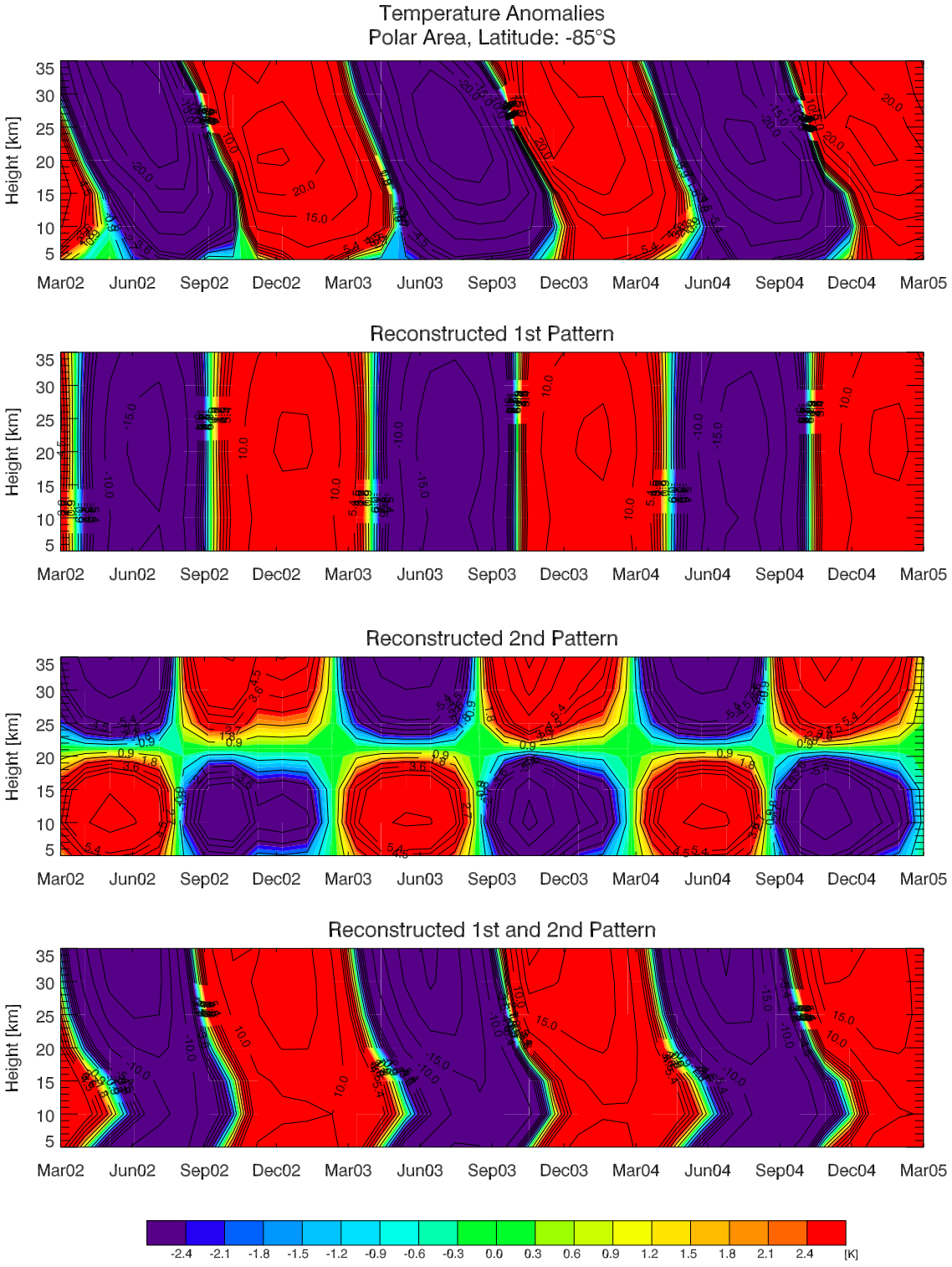

Fig. 30. Temperature anomalies (corrected for the 3-year mean value at each grid point), top, and reconstructed time series of the first (upper middle), the second (lower middle) and the combination of the first and the second (bottom) principal component/coefficient at 85°S (82.5°S to 87.5°S).

Low Latitudes

At low latitudes, similar to the PCA results of the south polar area, the first coefficient is associated with a uniform pattern (Fig. 31 bottom left), but inspecting the respective principal component (Fig. 31 top left) it can be seen that here we have another origin than seasonal cycle. This is confirmed after the reconstruction of the data by means of the first PC/coefficient (Fig. 32, upper middle panel) because the data do not show any seasonal cycle. Instead they show strong negative deviations from March 2002 to March 2003 and positive deviations from May 2003 to November 2003. Afterwards the reconstructed temperature anomalies generally stay comparatively small. The first pattern accounts for 52.4% of the total variance.

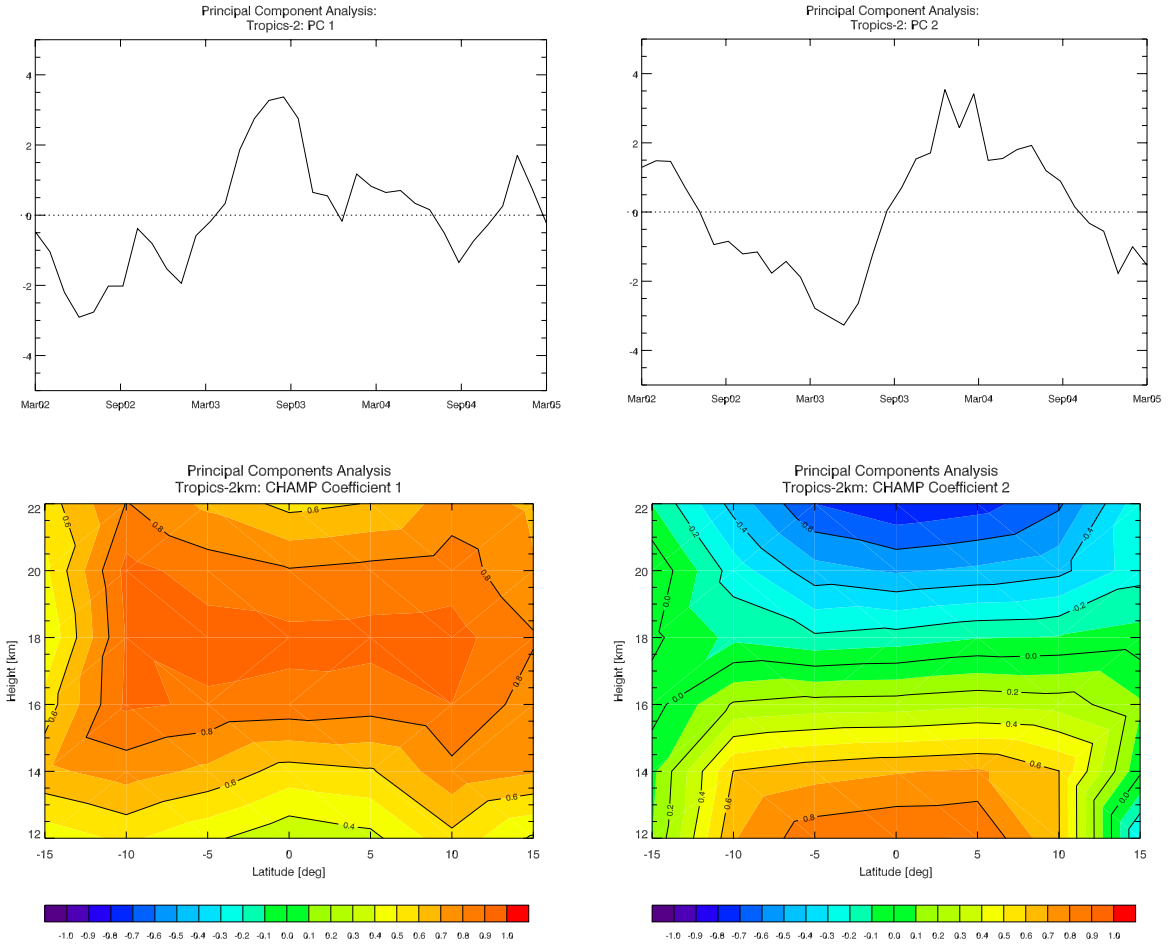

Fig. 31. First and second principal component (top) and corresponding coefficients (bottom) calculated by means of the correlation matrix from the low latitude dataset.

Figure 31 (right) depicts the second principal component (top) and its respective coefficient (bottom) calculated from the tropical dataset. The principal component shows a sinusoidal character with a frequency of more or less two years, a height dependent pattern can be recognized in the coefficient. In areas below and above a height of about 18 km there appears to be opposite sign. As can be seen in Fig. 32, lower middle panel, the second PC/coefficient is responsible for the resolution of the height dependent temporal behavior of the temperature anomalies. This 2nd pattern accounts for 22.0% of the total intrinsic variation.

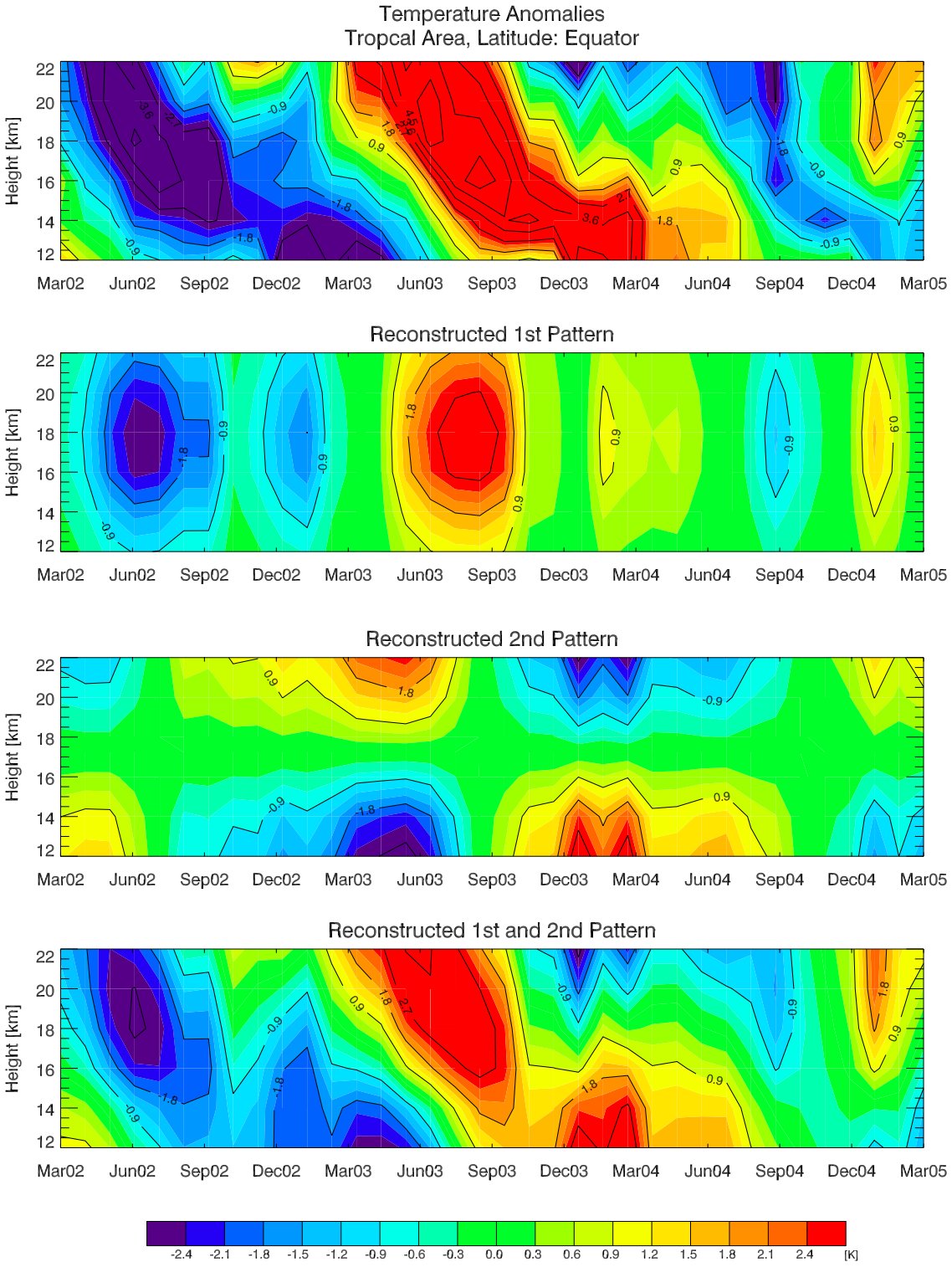

Fig. 32. Temperature anomalies (with prior elimination of the seasonal cycle), top, and reconstructed time series of the first and second principal component (two middle panels), as well as a combination of the first and second patterns (bottom) at the equator (2.5°S to 2.5°N).

In terms of geophysical interpretation, the detected phenomena can be clearly attributed to the so-called Quasi Biennial Oscillation (QBO), which dominates the inter-annual variability of the equatorial stratosphere within the height range of about 15 km and 50 km.

5 Conclusions and Outlook

The CHAMPCLIM results show that accurate zonal mean seasonal climatologies between 8 km and 30 km height can be obtained with data from a single RO receiver satellite. Future RO missions like the Taiwan/U.S. FORMOSAT-3/COSMIC constellation with 6 LEOs will provide thousands of RO profiles per day, but already now RO based climatologies have the potential to improve modern operational climatologies in regions where the data coverage and/or the vertical resolution and accuracy of RO data is superior to traditional data sources.

CHAMPCLIM activities will continue in the future. Climatologies of the atmospheric parameters beyond temperature, like refractivity and geopotential height, are currently being prepared and will be validated. Also the error models for all atmospheric parameters (refractivity, pressure, geopotential height, temperature) will be further developed. The next version of the WegCenter/CCR retrieval system will include wave-optics based tropospheric bending angle retrieval, and 1D-Var retrieval of temperature and humidity in the troposphere; also the error models will be amended by humidity error modeling.

Provision of the first CHAMPCLIM multi-year climatology datasets, including error estimates and tropopause parameters, to the scientific community is planned within 2006. The data are scheduled to be provided via the first version of the Climate Monitoring Center database and web portal of the WegCenter/UniGraz (CMC.WegCenter branch at the Wegener Center).

The results and the success of the CHAMPCLIM project furnished a pivotal starting point for long-term RO based climatologies. These will be continuously expanded with data from other RO missions in the years to come in order to monitor future climate variability and change in the atmosphere with unprecedented accuracy.

Acknowledgments

The authors gratefully acknowledge the GFZ Potsdam, Germany, for the provision of the CHAMP level 2 and level 3 correlative data, for technical support, especially provided by T. Schmidt, and for scientific discussion and advice provided by J. Wickert. We thank M. Fisher (ECMWF Reading) and A. Löscher (DMI Copenhagen) for providing error specifications for ECMWF analyses. J. Fritzer and J. Ramsauer provided helpful assistance regarding modification and use of the EGOPS software. We thank A. Simmons (ECMWF Reading), and S.S. Leroy (Harvard University) for valuable scientific discussions, and E. Manzini (INGV Bologna) and L. Kornblueh (MPI-M Hamburg) for their support and the provision of ECHAM5 data. Atmospheric analysis data were provided by ECMWF.
M. Borsche, A.K. Steiner, and A. Gobiet received financial support for the work from the CHAMPCLIM project funded by the Austrian Ministry for Traffic, Innovation, and Technology and managed under Contract No. ASAP-WV-203/05 of the Austrian Aeronautics and Space Agency (FFG-ALR). Furthermore, U. Foelsche, A.K. Steiner, and A. Gobiet received financial support from the START research award of G. Kirchengast funded by the Austrian Ministry for Education, Science, and Culture and managed under Program No. Y103-N03 of the Austrian Science Fund (FWF).

References

Anthes, R.A., C. Rocken, and Y. Kuo, Applications of COSMIC to Meteorology and Climate, *Terrestrial, Atmospheric and Oceanic Sciences*, 11(1), 115–156, 2000.

Bengtsson, L., S. Hagemann, and K.I. Hodges, Can climate trends be calculated from reanalysis data?, *J. Geophys. Res.*, 109, D11111, doi:10.1029/2004JD004536, 2004.

Borsche, M., A. Gobiet, A.K. Steiner, U. Foelsche, G. Kirchengast, T. Schmidt, and J. Wickert, Pre-Operational Retrieval of Radio Occultation based Climatologies, in: *Atmosphere and Climate: Studies by Occultation Methods* (U. Foelsche, G. Kirchengast, A.K. Steiner, eds.), Springer, Berlin-Heidelberg, in press, 2006a.

Borsche, M., U. Foelsche, A.K. Steiner, A. Gobiet, B.C. Lackner, B. Pirscher, and G. Kirchengast, Processing System for Provision of CHAMP Radio Occultation based Climatologies, *WegCenter Rep. for FFG-ALR No. 1/2006*, 41 p., Wegener Center, Univ. of Graz, Austria, 2006b.

Christy, J.R., and R.W. Spencer, Reliability of satellite data sets, *Science*, 301, 1046–1047, 2003.

Foelsche, U., G. Kirchengast, and A.K. Steiner, Global climate monitoring based on CHAMP/GPS radio occultation data, in *First CHAMP Mission Results for Gravity, Magnetic and Atmospheric Studies*, (C. Reigber et al., eds.), Springer, Berlin-Heidelberg, 397–407, 2003.

Foelsche, U., A. Gobiet, A. Löscher, G. Kirchengast, A.K. Steiner, J. Wickert, and T. Schmidt, The CHAMPCLIM project: An overview, in *Earth observation with CHAMP – results from three years in orbit*, (C. Reigber et al., eds.), Springer, Berlin-Heidelberg, 615–620, 2005.

Foelsche, U., A. Gobiet, A.K. Steiner, G. Kirchengast, M. Borsche, T. Schmidt, and J. Wickert Global Climatologies Based on Radio Occultation Data: The CHAMPCLIM Project, in: *Atmosphere and Climate: Studies by Occultation Methods* (U. Foelsche, G. Kirchengast, A.K. Steiner, eds.), Springer, Berlin-Heidelberg, in press 2006.

Fu, Q., C.M. Johanson, S.G. Warren, and D.J. Seidel, Contribution of stratospheric cooling to satellite-inferred tropospheric temperature trends, *Nature*, 429, 55–58, 2004.

Gobiet, A., and G. Kirchengast, Advancements of GNSS radio occultation retrieval in the upper stratosphere for optimal climate monitoring utility, *J. Geophys. Res.*, 109, D24110, doi:10.1029/2004JD005117, 2004.

Gobiet, A., A.K. Steiner, C. Retscher, U. Foelsche, and G. Kirchengast, Radio Occultation Data and Algorithms Validation Based on CHAMP/GPS Data, *Tech. Report for ASA No. 1/2004*, 50 p., Inst. for Geophys., Astrophys., and Meteorol., Univ. of Graz, Austria, 2004.

Gobiet, A., G. Kirchengast, J. Wickert, C. Retscher, D.-Y. Wang, and A. Hauchecorne, Evaluation of Stratospheric Radio Occultation Retrieval Using Data from CHAMP, MIPAS, GOMOS, and ECMWF Analysis Fields, in *Earth observation with CHAMP – Results from three years in orbit*, (C. Reigber, H. Lühr, P. Schwintzer, and J. Wickert, eds.), Springer, Berlin-Heidelberg, 531–536, 2005a.

Gobiet, A., U. Foelsche, A.K. Steiner, M. Borsche, G. Kirchengast, and J. Wickert, Climatological validation of stratospheric temperatures in ECMWF operational analyses with CHAMP radio occultation data, *Geophys. Res. Lett.*, 32, L12806, doi:10.1029/2005GL022617, 2005b.

Hajj, G.A., E.R. Kursinski, L.J. Romans, W.I. Bertiger, and S.S. Leroy, A Technical Description of Atmospheric Sounding by GPS occultation, *J. Atmos. Solar-Terr. Phys.*, 64, 451–469, 2002.

Hajj, G.A., C.O. Ao, P.A. Iijima, D. Kuang, E.R. Kursinski, A.J. Mannucci, T.K. Meehan, L.J. Romans, M. de la Torre Juarez, and T.P. Yunck, CHAMP and SAC-C atmospheric occultation results and intercomparisons, *J. Geophys. Res.*, 109, D06109, doi:10.1029/2003JD003909, 2004.

IPCC, Climate Change 2001 – The Scientific Basis. Contribution of WG I to the 3rd Assessment Report of the IPCC, (D.L. Albritton et al., eds.), Cambridge University Press, Cambridge, 2001.

Jolliffe, I.T., *Principal Component Analysis*, Springer series in statistics, New York, Berlin, Heidelberg, 2002.

Kirchengast, G., Occultations for Probing Atmosphere and Climate: Setting the Scene, in *Occultations for Probing Atmosphere and Climate*, (G. Kirchengast, U. Foelsche, A.K. Steiner, eds.), Springer, Berlin-Heidelberg, 1–8, 2004.

Kirchengast, G., J. Fritzer, and J. Ramsauer, End-to-end GNSS Occultation Performance Simulator Version 4 (EGOPS4) Software User Manual (Overview and Reference Manual), *Techn. Report for ESA/ESTEC*, Inst. for Geophys., Astrophys., and Meteorol., Univ. of Graz, Austria, No. 3/2002.

Kursinski, E.R., G.A. Hajj, W.I. Bertiger, S.S. Leroy, T.K. Meehan, L.J. Romans, J.T. Schofield, D.J. McCleese, W.G. Melbourne, C.L. Thornton, T.P. Yunck, J.R. Eyre, and R.N. Nagatani, Initial results of radio occultation of Earth's atmosphere using the global positioning system, *Science*, 271, 1107–1110, 1996.

Kursinski, E.R., G.A. Hajj, J.T. Schofield, R.P. Linfield, and K.R. Hardy, Observing Earth's Atmosphere with Radio Occultation Measurements Using the Global Positioning System, *J. Geophys. Res*., 102, 23429–23465, 1997.

Lackner, B.C., and B. Pirscher, Climate Diagnostics in Radio Occultation Temperature Climatologies of CHAMP and ECMWF, *WegCenter Scientific Report* No. 7/2005, Wegener Center for Climate and Global Change, Univ. of Graz, 2005.

Leroy, S.S., The measurement of geopotential heights by GPS radio occultation, *J. Geophys. Res.*, 102, 6971–6986, 1997.

Leroy, S.S., J.A. Dykema, and J.G. Anderson, Climate Benchmarking Using GNSS Occultation, in: *Atmosphere and Climate: Studies by Occultation Methods* (U. Foelsche, G. Kirchengast, A.K. Steiner, eds.), Springer, Berlin-Heidelberg, in press 2006.

Loiselet, M., N. Stricker, Y. Menard, and J.-P. Luntama, GRAS – MetOp's GPS-based atmospheric sounder, *ESA Bull.*, 102, 38–44, 2000.

Löscher, A., U. Foelsche, and G. Kirchengast, CHAMP Radio Occultation Data Assimilation into ECMWF Fields for Global Climate Analyses, *WegCenter Rep. for FFG-ALR No. 2/2006*, 57 p., Wegener Center, Univ. of Graz, Austria, 2006.

Mears, C., M. Schabel, and F. J. Wentz, A reanalysis of the MSU channel 2 tropospheric temperature record, *J. Clim.*, 16, 3650–3664, 2003.

Poli, P., Assimilation of GNSS radio occultation data into numerical weather prediction, in: *Atmosphere and Climate: Studies by Occultation Methods* (U. Foelsche, G. Kirchengast, A.K. Steiner, eds.), Springer, Berlin-Heidelberg, in press 2006.

Reyment, R.A., and K.G. Jöreskog, *Applied Factor Analysis in the Natural Science*, Cambridge University Press, Cambridge, 1993.

Rocken, C., R. Anthes, M. Exner, D. Hunt, S. Sokolovskiy, R. Ware, M. Gorbunov, W. Schreiner, D. Feng, B. Herman, Y.H. Kuo, and X. Zou, Analysis and Validation of GPS/MET Data in the Neutral Atmosphere, *J. Geophys. Res.*, 102(D25), 29849–29866, 1997.

Rocken, C., Y. Kuo, W.S. Schreiner, D. Hunt, S. Sokolovskij, and C. McCormick, COSMIC System Description. *Terr., Atmos. and Oceanic Sci.* 11: 21–52, 2000.

Roeckner E, G. Baeuml, L. Bonaventura, R. Brokopf, M. Esch, M. Giorgetta, S. Hagemann, I. Kirchner, L. Kornblueh, E. Manzini, A. Rhodin, U. Schlese, U. Schulzweidea, and A. Tompkins, The atmospheric general circulation model ECHAM5 Part 1. *MPI Rep*, 349, Max-Planck-Inst f Meteorol, Hamburg, Germany, 2003.

Smith, E.K., S. Weintraub, The constants in the equation for atmospheric refractive index at radio frequencies. *Proc of the IRE* 41, 1035–1037, 1953.

Steiner, A.K., and G. Kirchengast, Error analysis for GNSS radio occultation data based on ensembles of profiles from end-to-end simulations, *J. Geophys. Res.*, 110(D15307), doi:10.1029/2004JD005251, 2005.

Steiner, A.K., G. Kirchengast, and H.P. Ladreiter, Inversion, Error Analysis and Validation of GPS/MET Occultation Data, *Ann. Geophys*., 17, 22–138, 1999.

Steiner, A.K., G. Kirchengast, U. Foelsche, L. Kornblueh, E. Manzini, and L. Bengtsson, GNSS Occultation Sounding for Climate Monitoring, *Phys. Chem. Earth A*, 26, 13–124, 2001.

Steiner, A.K., A. Gobiet, U. Foelsche, G. Kirchengast, Radio occultation data processing advancements for optimizing climate utility. *IGAM/Uni Graz Tech Rep for ASA*, No. 3/2004.

Steiner, A.K., A. Löscher, and G. Kirchengast, Error Characteristics of Refractivity Profiles Retrieved from CHAMP Radio Occultation Data, in: *Atmosphere and Climate: Studies by Occultation Methods* (U. Foelsche, G. Kirchengast, A.K. Steiner, eds.), Springer, Berlin-Heidelberg, in press 2006.

Syndergaard, S., Retrieval analysis and methodologies in atmospheric limb sounding using the GNSS radio occultation technique, *DMI Sci. Rep*., 99-6, Danish Meteorol. Inst., Copenhagen, Denmark, 131 pp, 1999.

Vedel, H., and M. Stendel, On the direct use of GNSS refractivity measurements for climate monitoring, in *Proceedings from the 4'th Oersted International Science Team Conference (OIST-4)*, (P. Stauning et al., eds.), 275–278, Danish Meteorological Institute, Copenhagen, DK, 2003.

Vinnikov, K.Y., and N.C. Grody, Global warming trend of mean tropospheric temperature observed by satellites, *Science*, 302, 269–272, 2003.

Ware, R., M. Exner, D. Feng, M. Gorbunov, K. Hardy, B. Herman, Y. Kuo, T. Meehan, W. Melbourne, C. Rocken, W. Schreiner, S. Sokolovskiy, F. Solheim, X. Zou, R. Anthes, S. Businger, and K. Trenberth, GPS Sounding of the atmosphere from Low Earth Orbit: Preliminary results, *Bull. Am. Meteorol. Soc*., 77, 19–40, 1996.

Wickert, J., C. Reigber, G. Beyerle, R. König, C. Marquardt, T. Schmidt, L. Grunwaldt, R. Galas, T. K. Meehan, W.G. Melbourne, and K. Hocke, Atmospheric sounding by GPS radio occultation: First results from CHAMP, *Geophys. Res. Lett.*, 28, 3263–3266, 2001.

Wickert, J., T. Schmidt, G. Beyerle, R. König, C. Reigber, and N. Jakowski, The radio occultation experiment aboard CHAMP: Operational data analysis and validation of vertical atmospheric profiles, *J. Meteorol. Soc. Japan*, 82, 381–395, 2004.

WMO, Definition of the tropopause, in *WMO Bull*.,6, 1957.

Wu, B.-H., V. Chu, P. Chen, and T. King, FORMOSAT-3/COSMIC science mission update, *GPS solutions*, 9, 111–121, doi:10.1007/s10291-005-0140-z, 2005.

Appendix A: Monthly Climatologies for a Full Year

In this Appendix we present monthly-mean, zonal-mean CHAMP dry temperature fields together with the corresponding error estimates for each single month of a complete year. The geographical distribution of the CHAMP RO events during each month of the year 2003 is shown in Fig. A.1. CHAMP dry temperature climatologies are displayed in Fig. A.2 and the corresponding reference ECMWF fields in Fig. A.3. The systematic difference between CHAMP and ECMWF (biases between the datasets) is shown in Fig. A.4, the CHAMP sampling error in Fig. A.5, and the climatological difference (CHAMP climatology minus ECMWF reference climatology) in Fig. A.6, respectively.

This overview serves as a small atlas for readers with closer interest in the subject. By way of a full example year it illustrates in more detail the wealth of information in the CHAMPCLIM climatology products derived from CHAMP radio occultation observations.

CHAMP RO Event Distribution – Year 2003

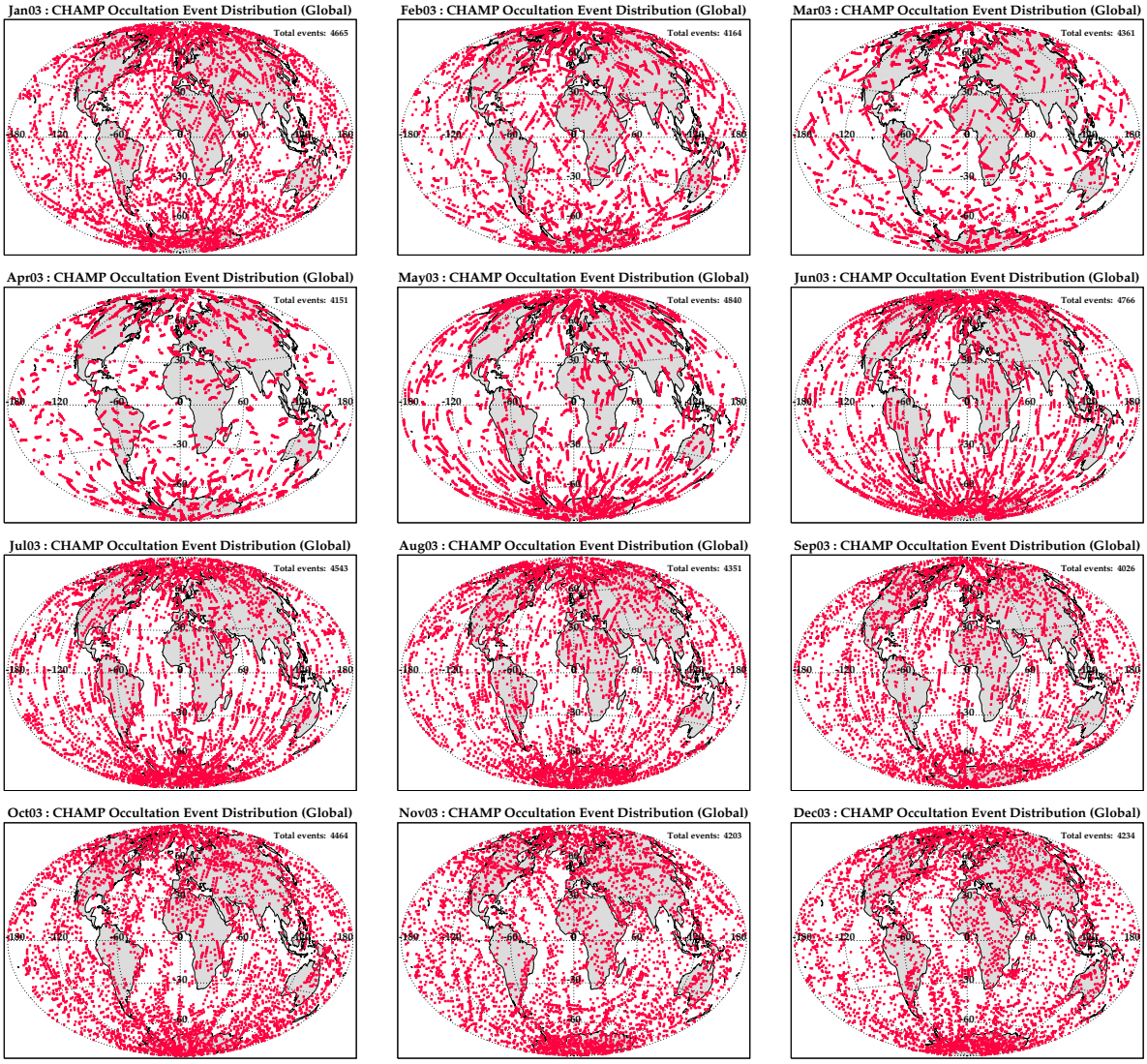

Fig. A.1. Geographical distribution of CHAMP RO events from January 2003 to December 2003.

CHAMP Temperature Climatologies – Year 2003

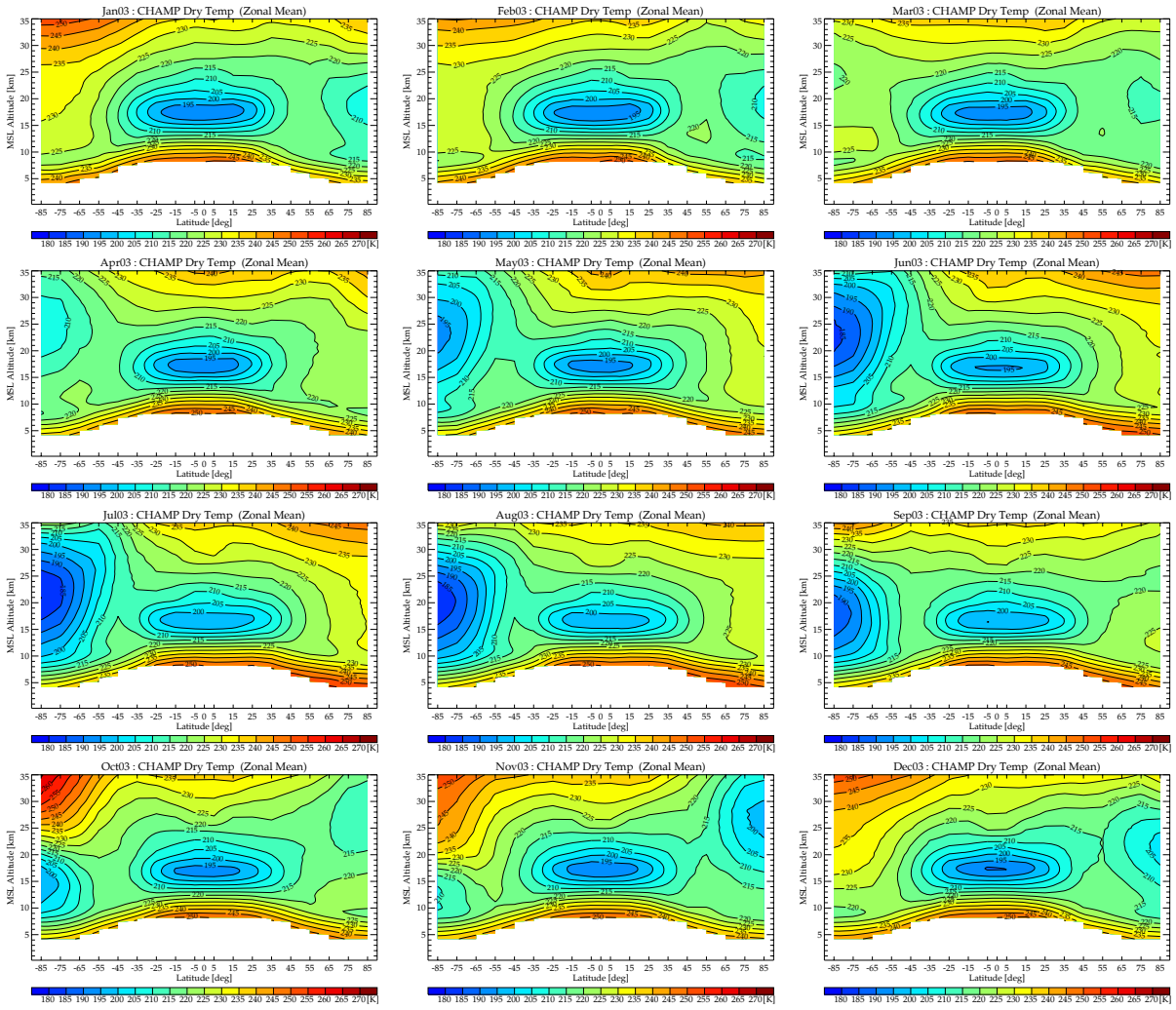

Fig. A.2. CHAMP dry temperature climatologies; monthly-mean, zonal-mean climatologies from January 2003 to December 2003.

ECMWF Temperature Climatologies – Year 2003

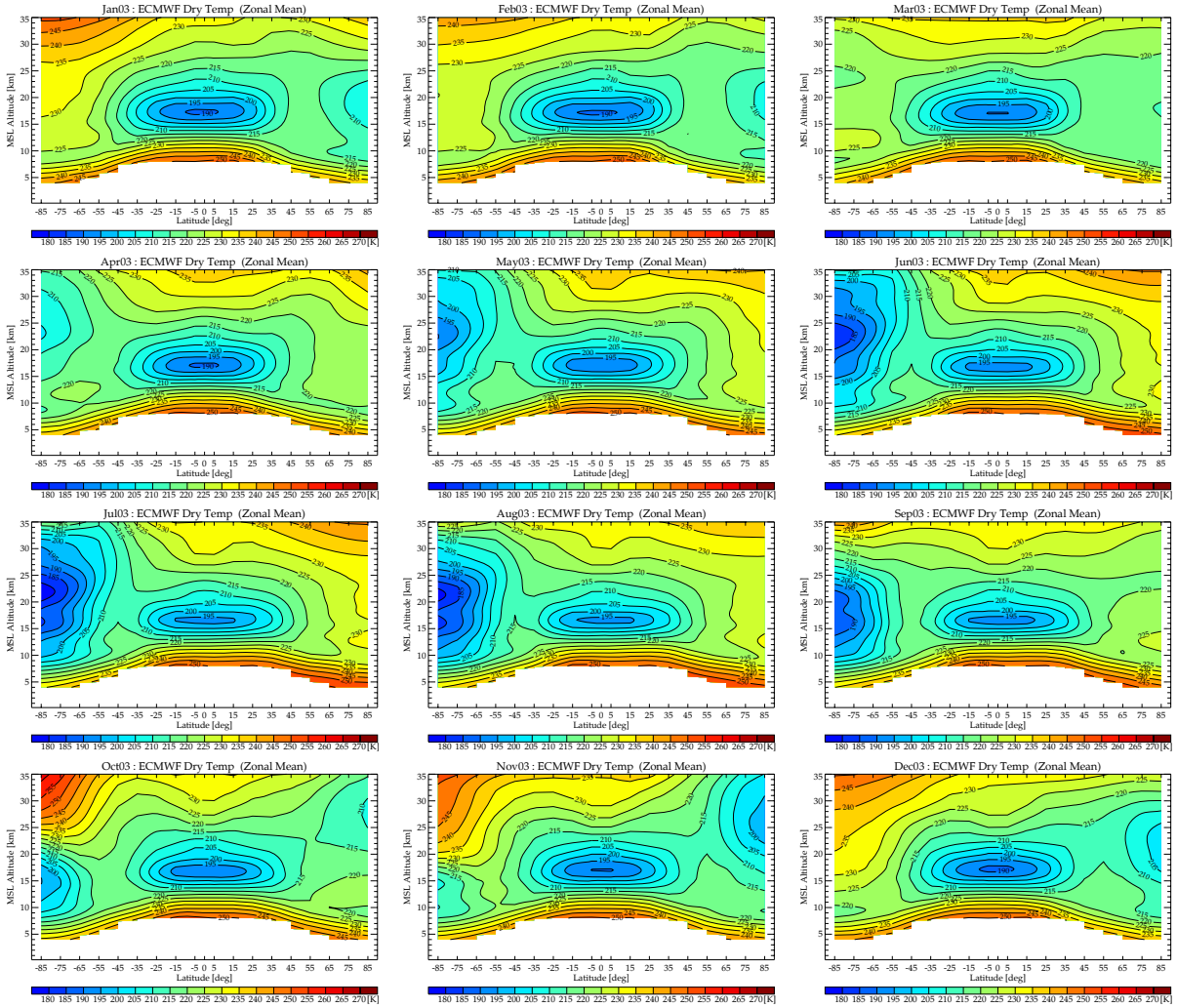

Fig. A.3. ECMWF dry temperature climatologies; monthly-mean, zonal-mean climatologies from January 2003 to December 2003.

CHAMP Temperature Climatologies: Systematic Difference to ECMWF

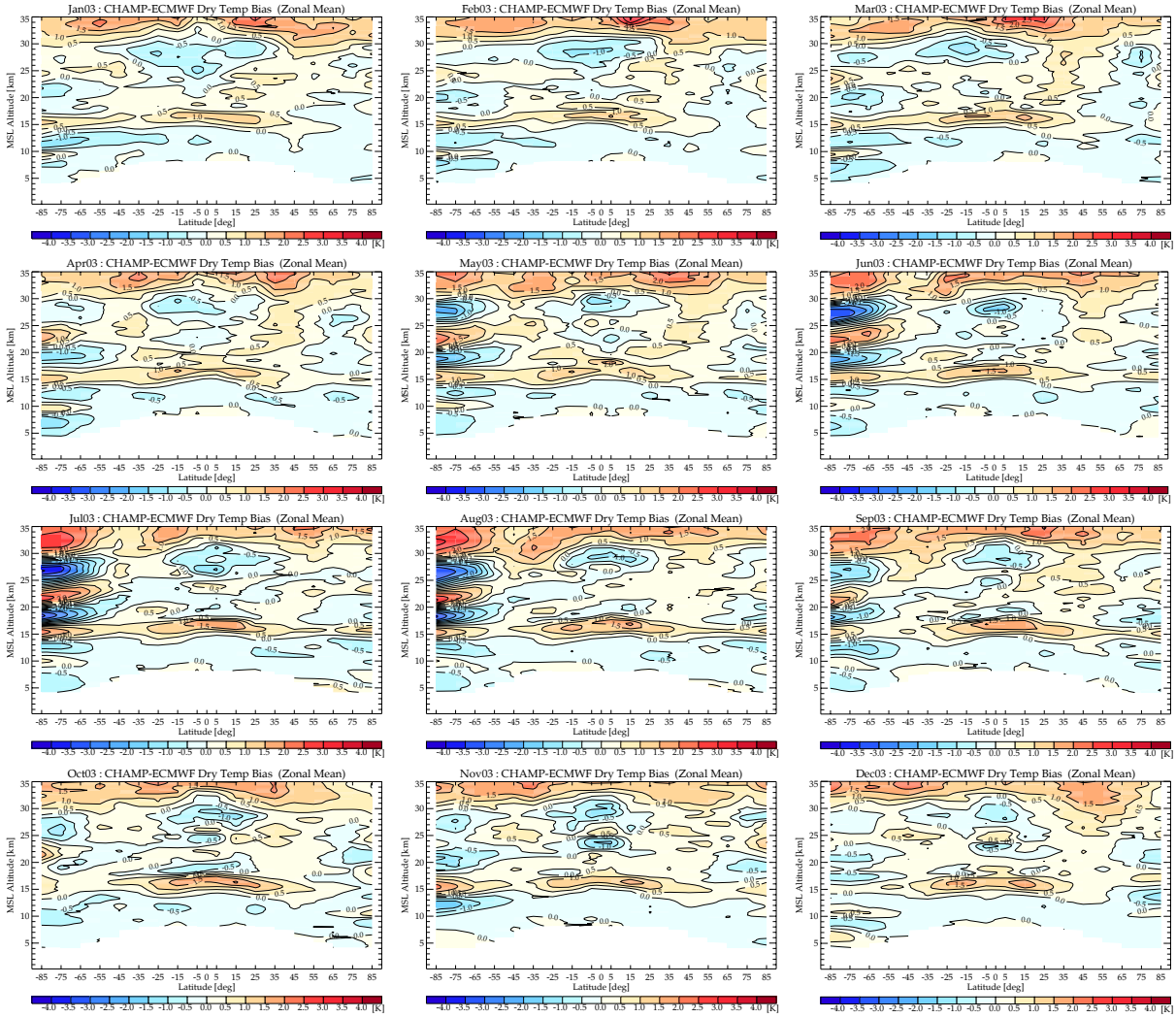

Fig. A.4. CHAMP dry temperature, systematic difference to ECMWF with the latter as reference (bias between the two datasets); monthly-mean, zonal-mean datasets from January 2003 to December 2003.

CHAMP Temperature Climatologies: Sampling Error

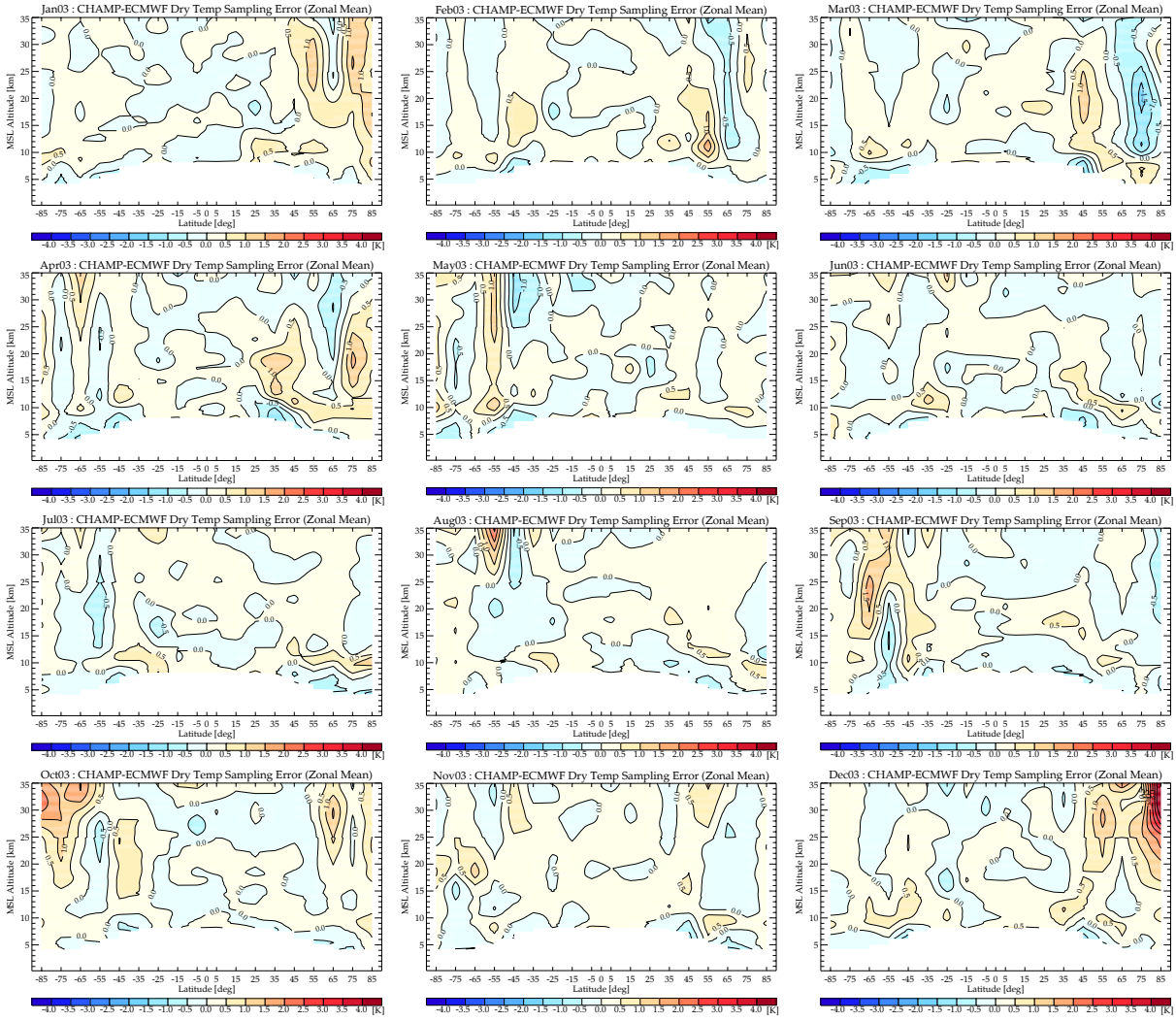

Fig. A.5. CHAMP dry temperature sampling error (ECMWF climatology derived from RO co-located ECMWF profiles minus ECMWF reference climatology); monthly-mean, zonal-mean datasets from January 2003 to December 2003.

CHAMP Temperature Climatologies: Climatological Difference

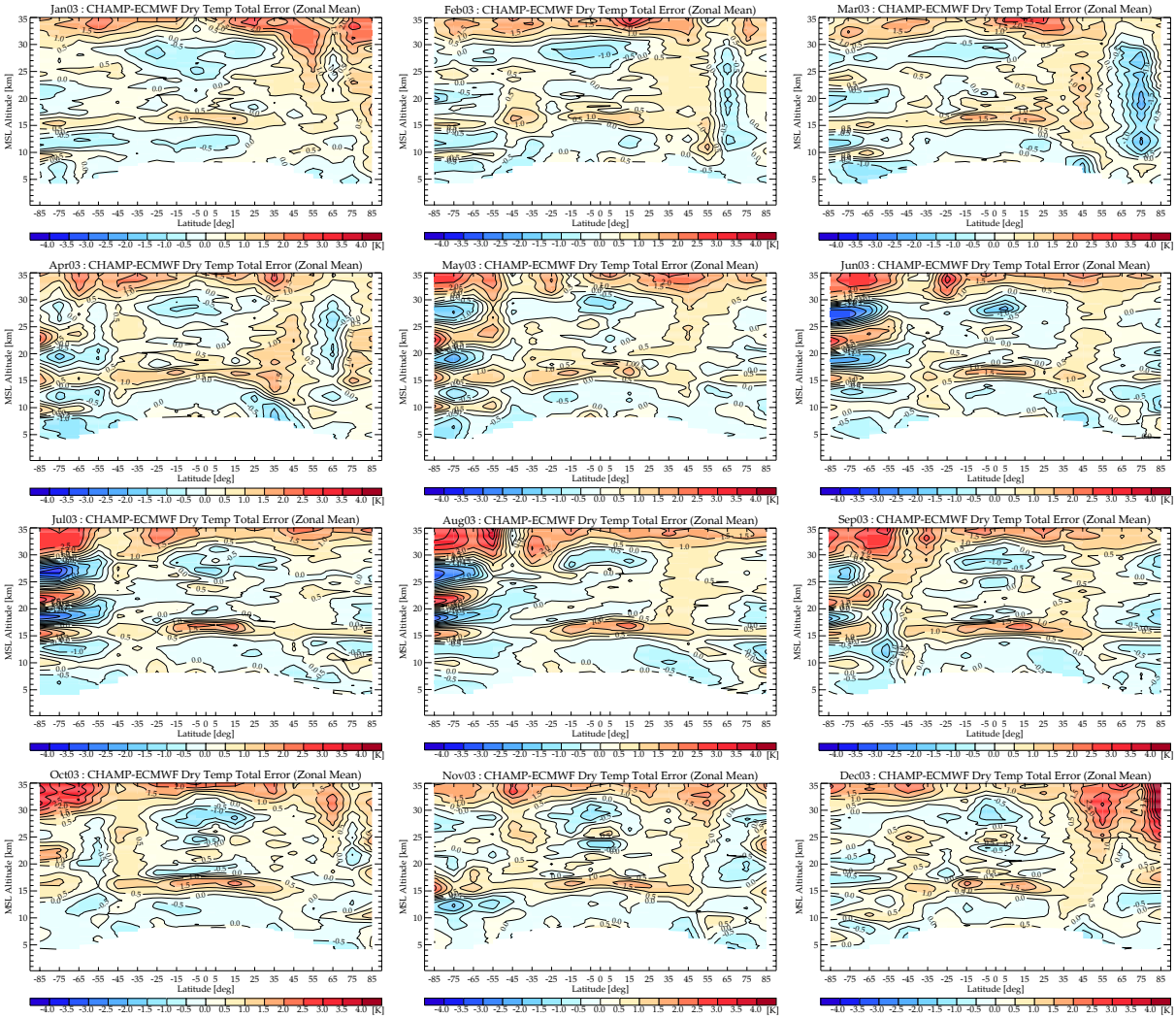

Fig. A.6. CHAMP dry temperature climatological difference (CHAMP derived climatology minus ECMWF reference climatology); monthly-mean, zonal-mean datasets from January 2003 to December 2003.

Ω end of document Ω